Article

Ligand-Stabilized Aromatic Three-Membered Gold Rings and Their Sandwichlike Complexes

Athanassios C. Tsipis, and Constantinos A. Tsipis

J. Am. Chem. Soc., **2005**, 127 (30), 10623-10638• DOI: 10.1021/ja051415t • Publication Date (Web): 12 July 2005

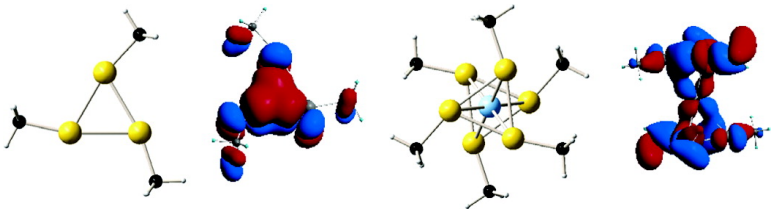

J|A|C|S
ARTICLES
Published on Web 07/12/2005

Ligand-Stabilized Aromatic Three-Membered Gold Rings and Their Sandwichlike Complexes

Athanassios C. Tsipis[†] and Constantinos A. Tsipis*[,‡]

Contribution from the Laboratory of Inorganic and General Chemistry, Department of Chemistry, University of Ioannnina, Ioannina 451 10, Greece, and Laboratory of Applied Quantum Chemistry, Faculty of Chemistry, Aristotle University of Thessaloniki, 541 24 Thessaloniki, Greece

Received March 5, 2005; E-mail: tsipis@chem.auth.gr

Abstract: Electronic structure calculations (DFT) suggest that ligand-stabilized three-membered gold(I) rings constituting the core structure in a series of *cyclo*-$Au_3L_nH_{3-n}$ ($L = CH_3$, NH_2, OH and Cl; $n = 1, 2, 3$) molecules exhibit aromaticity, which is primarily due to 6s and 5d cyclic electron delocalization over the triangular Au_3 framework (s- and d-orbital aromaticity). The aromaticity of the novel triangular gold(I) isocycles was verified by a number of established criteria of aromaticity. In particular, the nucleus-independent chemical shift, NICS(0), the upfield changes in the chemical shifts for Li^+, Ag^+, and Tl^+ cations over the Au_3 ring plane, and their interaction with electrophiles (e.g., H^+, Li^+, Ag^+, and Tl^+) are indicative for the aromaticity of the three-membered gold(I) rings. Interestingly, unlike the respective substituted derivatives of cyclopropenium cation and the bora-cyclopropene carbacyclic analogues, the aromatic Au_3 rings, although exhibit comparable diatropicity, react with electrophiles in a different way affording 1:1 and 2:1 sandwichlike complexes. The bonding in the three-membered gold(I) rings is characterized by a common ring-shaped electron density, more commonly seen in aromatic organic molecules and in "all-metal" aromatics, such as the *cyclo*-$[Hg_3]^{4-}$ tetraanion. Moreover, the cation$-\pi$ interactions in the 1:1 and 1:2 sandwichlike complexes formed upon reacting the Au_3 rings with electrophiles, depending on the nature of the cation, are predicted to be predominantly electrostatic (Li^+, Tl^+) or covalent (H^+, Ag^+). The 1:2 complexes constitute a new class of sandwichlike complexes, which are expected to have novel properties and applications.

Introduction

Coinage metal atoms have a marked tendency to form aggregates with metal−metal distances shorter than the sum of their van der Waals radii (copper(I) = 140 pm, Ag(I) = 172 pm, and gold(I) = 166 pm).[1] Particularly abundant are both the bare gold(I) clusters and the ligand-stabilized gold(I) complexes which tend to form 1D-, 2D-, or 3D-structures based on Au(I)−Au(I) interactions of comparable strength to that of the hydrogen bonds.[2] Interestingly, the lowest energy structures of all bare gold(I) clusters with up to eight gold(I) atoms in their ground states correspond to the perfectly planar 2D-isomers, the planar-to-nonplanar turnover occurring between Au_6 and Au_8.[3] Neutral and anionic gold clusters favoring 2D-structures are very common building "bricks" for nanostructured materials, electronic devices, and nanocatalytic systems.[4−9] Moreover, the trimers are known to play a special role in coinage metal halides in the gas phase: an amazing common property of all these compounds is the unusual abundance of trimers in their vapor.[10−12] The cyclic trinuclear gold(I) complexes involving three-membered gold(I) rings were found in a variety of gold(I) polynuclear complexes studied so far.[13] Thus, the Au_3 triangle consists of the core structure of carbeniate [Au(μ-C,N−R′N=COR)]$_3$ (R = aryl or alkyl) and benzimidazolate [Au(μ-C^2,N^3-bzim)]$_3$ (bzim = 1-benzimidazolate) complexes.[14] Most important is the tendency of the Au_3 triangle containing molecules to stack with a variety of organic and organometallic π acid molecules, such as the [Hg(μ-C,C−C_6F_4)]$_3$ complex[15,16] and nitro-substituted fluorenones[17,18] and interact with metal

[†] University of Ioannnina.
[‡] Aristotle University of Thessaloniki.

(1) http://www.webelements.com.
(2) Schmidbaur, H. *Gold. Bull.* **2000**, *33*, 3.
(3) Olson, R. M.; Varganov, S.; Gordon, M. S.; Metiu, H.; Chretien, S.; Piecuch, P.; Kowalski, K.; Kucharski, S. A.; Musial, M. *J. Am. Chem. Soc.* **2005**, *127*, 1049.
(4) Alivisatos, A. P. *Science* **1996**, *271*, 933.
(5) Valden, M.; Lai, X.; Goodman, D. W. *Science* **1998**, *281*, 1647.
(6) Häkkinen, H.; Barnett, R. N.; Landman, U. *Phys. Rev. Lett.* **1999**, *82*, 3264.
(7) Häkkinen, H.; Landman, U. *J. Am. Chem. Soc.* **2001**, *123*, 9704.
(8) Nam, J.-M.; Thaxton, C. S.; Mirkin, C. A. *Science* **2003**, *301*, 1884.
(9) Remacle, F.; Kryachko, E. S. In *Advances in Quantum Chemistry*; Brandas, E., Kryachko, E. S., Eds.; Elsevier: 2004; Vol. 47, p 509 and references therein.
(10) Bertolus, M.; Brenner, V.; Millie, P. *Eur. Phys. J.* **2000**, *D11*, 387.
(11) L'Hermite, J.-M.; Rabilloud, F.; Labastie, P.; Spiegelman, F. *Eur. Phys. J.* **2001**, *D16*, 77.
(12) L'Hermite, J.-M.; Rabilloud, F.; Marcou, L.; Labastie, P. *Eur. Phys. J.* **2001**, *D14*, 323.
(13) Burini, A.; Mohamed, A. A.; Fackler, J. P., Jr. *Comm. Inorg. Chem.* **2003**, *24*, 253.
(14) Fackler, J. P., Jr. *Inorg. Chem.* **2002**, *41*, 6959 and references therein.
(15) Burini, A.; Fackler, J. P., Jr.; Galassi, R.; Grant, T. A.; Omary, M. A.; Rawashdeh-Omary, M. A.; Pietroni, B. R.; Staples, R. J. *J. Am. Chem. Soc.* **2000**, *122*, 11264.
(16) Burini, A.; Fackler, J. P., Jr.; Galassi, R.; Macchioni, A.; Omary, M. A.; Rawashdeh-Omary, M. A.; Pietroni, B. R.; Sabatini, S.; Zuccaccia, C. *J. Am. Chem. Soc.* **2002**, *124*, 4570.
(17) Olmstead, M. M.; Jiang, F.; Attar, S.; Balch, A. L. *J. Am. Chem. Soc.* **2001**, *123*, 3260.
(18) Balch, A. L.; Olmstead, M. M.; Vickery, J. C. *Inorg. Chem.* **1999**, *38*, 3494.

10.1021/ja051415t CCC: $30.25

cations, such as Ag(I) and Tl(I), to form "sandwich" complexes analogous to metallocenes.[19] Interestingly, some of these complexes display the novel property of solvoluminescence.[14,17,18] The Au_3 triangle capped with O, N, or S donor atoms consists of also the core structure in a series of complexes formulated as $[XAu_3]^+$ and $\{X[Au(PR_3)]_3\}^+$ (X = O, N, or S).[20−28] The aurophilic interactions in these complexes have exhaustively been investigated very recently[29] by quasi-relativistic DFT calculations. Aurophilic interactions are clearly shown in the Au_3 triangle of the phosphido-bridged trinuclear gold(I) complex $[Au(\mu\text{-}PIs_2)]_3$ (Is = 2,4,6,-(*i*-Pr)$_3C_6H_2$)) with Au−Au distances ranging from 306.6 to 309.7 pm.[30]

Continuing our interest on the exploitation of aromatic metallic rings[31,32] analogous to the classical aromatic carbon rings in organic chemistry, we report herein on novel ligand-stabilized three-membered aromatic gold rings and compare their aromaticity, primarily arisen from both strong *n*s and $(n-1)$d orbital contributions (σ_s-, σ_d-, π_d-, and δ_d-aromaticity), to the traditional organic aromaticity due to 2p orbital contributions (π_p-aromaticity). In effect, what we want to address here is the stability, aromaticity, molecular structure, and related properties of substituted derivatives of the aromatic three-membered hydrogold(I) isocycles formulated as $Au_3L_nH_{3-n}$(L = CH_3, NH_2, OH, and Cl; n = 1, 2, 3). Moreover, their interaction with metal cations (electrophiles), such as Li^+, Ag^+, and Tl^+, has also been studied. The effect of the substituents on the aromatic character of the Au_3 rings is also a main concern of the present work.

Theoretical Methods

In view of the good performance of density functional theory (DFT), we were instigated to perform DFT calculations at the B3LYP level of theory on all of the compounds we studied using the GAUSSIAN03 program suite.[33] The geometries of all species were fully optimized at the Becke's three-parameter hybrid functional[34,35] combined with the Lee−Yang−Parr[36] correlation functional abbreviated as the B3LYP level of density functional theory, using the LANL2DZ basis set for the Au atoms and the 6-31G(d,p) basis set for the rest of the nonmetal atoms. Moreover, one additional *f*-type polarization function ($\alpha_f = 0.75$) is implemented for the Au atoms. It has been found that such polarization functions are required for precisely describing the aurophilic interaction.[37−39] We will denote the computational approach used as B3LYP/LANL2DZ+*f*(Au)∪6-31G**(L). Full geometry optimization was performed for each structure using Schlegel's analytical gradient method,[40] and the attainment of the energy minimum was verified by calculating the vibrational frequencies that result in absence of imaginary eigenvalues. All the stationary points have been identified for minimum (number of imaginary frequencies NIMAG = 0) or transition states (NIMAG = 1). The vibrational modes and the corresponding frequencies are based on a harmonic force field. This was achieved with the SCF convergence on the density matrix of at least 10^{-9} and the rms force less than 10^{-4} au. All bond lengths and bond angles were optimized to better than 0.001 Å and 0.1°, respectively. The computed electronic energies, the enthalpies of reactions, $\Delta_R H_{298}$, and the free energies, ΔG_{298}, were corrected to constant pressure and 298 K, for zero-point energy (ZPE) differences and for the contributions of the translational, rotational, and vibrational partition functions. The natural bond orbital (NBO) population analysis was performed using Weinhold's methodology.[41,42] Magnetic shielding tensors have been computed with the GIAO (gauge-including atomic orbitals) DFT method[43,44] as implemented in the GAUSSIAN03 series of programs[33] employing the B3LYP level of theory. Nucleus-independent chemical shift (NICS) values were computed at the B3LYP/LANL2DZ level according to the procedure described by Schleyer et al.[45] The magnetic shielding tensor element was calculated for a ghost atom located at the center of the ring. Negative (diatropic) NICS values indicate aromaticity, while positive (paratropic) values imply antiaromaticity.

Results and Discussion

Equilibrium Geometries of the *cyclo*-$Au_3L_nH_{3-n}$ (L = CH_3, NH_2, OH, and Cl; n = 1, 2, 3) Compounds. Stationary point geometries of the *cyclo*-$Au_3L_nH_{3-n}$ (L = CH_3, NH_2, OH and Cl; n = 1, 2, 3) molecules computed at the B3LYP/LANL2DZ+*f*(Au)∪6-31G**(L) level of theory are presented in Figures 1 and 2.

A thorough search of the potential energy surfaces (PES), using different starting geometries, revealed that all *cyclo*-$Au_3L_nH_{3-n}$ clusters, except the methyl-substituted derivatives, are fluxional molecules adopting two different configurations with respect to the bonding mode of the stabilizing ligands. The global minima (Figure 1) correspond to the structures involving bridging stabilizing ligands L, while the structures involving terminal stabilizing ligands correspond to local minima (Figure 2). It should be noted that the methyl-substituted derivatives adopt only the structures with terminal methyl and hydride ligands (Figure 1). The relative energies of the local minimum structures with respect to the global minimum structures are also shown in Figure 2.

It can be seen that formation of the almost symmetrical hydrido-, amido-, hydroxo-, and chloro-bridges stabilizes the cyclic trinuclear clusters. It is important to notice that the first base-free homoleptic gold(I) disilyl-amide, $[\{Au(\mu\text{-}N(SiMe_3)_2\}_4]$, synthesized and structurally characterized recently[46] adopts the more stable configuration with symmetrical bridging amide ligands. Similarly, the unusually abundant trimers in the vapors of silver bromide adopt also the most stable configuration with almost symmetrical bridging bromide ligands.[11,12] To understand the higher stability of the trinuclear gold(I) clusters upon

(19) Burini, A.; Bravi, R.; Fackler, J. P., Jr.; Galassi, R.; Grant, T. A.; Omary, M. A.; Pietroni, B. R.; Staples, R. J. *Inorg. Chem.* **2000**, *39*, 3158.
(20) Angermaier, K.; Schmidbaur, H. *Chem. Ber.* **1994**, *127*, 2387.
(21) Schmidbaur, H.; Kolb, A.; Zeller, E.; Schier, A.; Beruda, H. *Z. Anorg. Allg. Chem.* **1993**, *619*, 1575.
(22) Angermaier, K.; Schmidbaur, H. *Acta Crystallogr. C* **1995**, *51*, 1793.
(23) Angermaier, K.; Schmidbaur, H. *Inorg. Chem.* **1994**, *33*, 2069.
(24) Schmidbaur, H.; Zeller, E.; Weidenhiller, G.; Steigelmann, O.; Beruda, H. *Inorg. Chem.* **1992**, *31*, 2370.
(25) Schmidbaur, H.; Gabbai, F. P.; Schier, A.; Riede, J. *Organometallics* **1995**, *14*, 4969.
(26) Bachman, R. E.; Schmidbaur, H. *Inorg. Chem.* **1992**, *35*, 1399.
(27) Schmidbaur, H.; Kolb, A.; Bissinger, P. *Inorg. Chem.* **1992**, *31*, 4370.
(28) Yang, Y.; Ramamoorthy, V.; Sharp, P. R. *Inorg. Chem.* **1993**, *32*, 1946.
(29) Wang, S.-G.; Schwarz, W. H. E. *J. Am. Chem. Soc.* **2004**, *126*, 1266.
(30) Stefanescu, D. M.; Yuen, H. F.; Glueck, D. S.; Golen, J. A.; Zakharov, L. N.; Incarvito, C. D.; Rheingold, A. L. *Inorg. Chem.* **2003**, *42*, 8891.
(31) Tsipis, A. C.; Tsipis, C. A. *J. Am. Chem. Soc.* **2003**, *125*, 1136.
(32) Tsipis, A. C.; Karagiannis, E. E.; Kladou, P. F.; Tsipis, A. C. *J. Am. Chem. Soc.* **2004**, *126*, 12916.
(33) Frisch, M. J. T.; et al. *Gaussian 03*, revision B. 02; Gaussian, Inc.: Pittsburgh, PA, 2003. See Supporting Information for remaining 80 authors.
(34) Becke, A. D. *J. Chem. Phys.* **1992**, *96*, 215.
(35) Becke, A. D. *J. Chem. Phys.* **1993**, *98*, 5648.
(36) Lee, C.; Yang, W.; Parr, R. G. *Phys. Rev. Lett.* **1998**, *B 37*, 785.
(37) Pyykkö, P.; Runeberg, N.; Mendizabal, F. *Chem.−Eur. J.* **1997**, *3*, 1451.
(38) Pyykkö, P.; Mendizabal, F. *Chem.−Eur. J.* **1997**, *3*, 1458.
(39) Pyykkö, P. *Chem. Rev.* **1997**, *97*, 597.
(40) Schlegel, H. B. *J. Comput. Chem.* **1982**, *3*, 214.
(41) Reed, A. E.; Curtiss, L. A.; Weinhold, F. *Chem. Rev.* **1988**, *88*, 899.
(42) Weinhold, F. In *The Encyclopedia of Computational Chemistry*; Schleyer, P. v. R., Ed.; John Wiley & Sons: Chichester, 1998; pp 1792−1811.
(43) Ditchfield, R. *Mol. Phys* **1974**, *27*, 789.
(44) Gauss, J. *J. Chem. Phys.* **1993**, *99*, 3629.
(45) Schleyer, P. v. R.; Maerker, C.; Dransfeld, A.; Jiao, H.; Hommes, N. J. R. v. R. *J. Am. Chem. Soc.* **1996**, *118*, 6317.
(46) Bunge, S. D.; Just, O.; Rees, W. S., Jr. *Angew. Chem., Int. Ed.* **2000**, *39*, 3082.

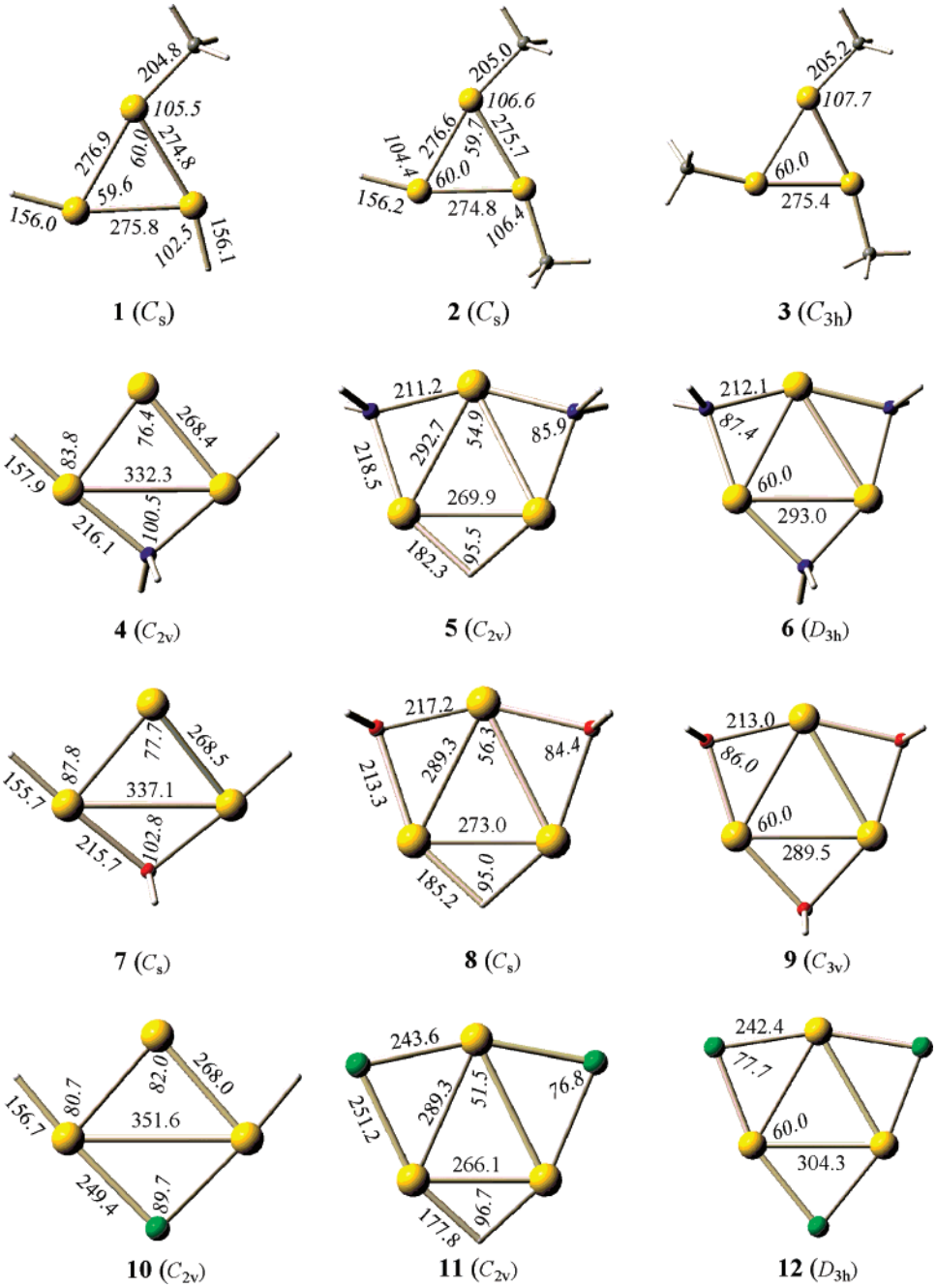

Figure 1. Equilibrium geometries (bond lengths in pm, angles in deg) of the *cyclo*-$Au_3L_nH_{3-n}$ (L = CH_3, NH_2, OH, and Cl; n = 1, 2, 3) molecules corresponding to global minima in the PES computed at the B3LYP/LANL2DZ+*f*(Au)∪6-31G**(L) level of theory.

formation of symmetrical peripheral bridges around the Au_3 triangle, we looked whether the peripheral isosceles triangles formed possess aromatic character. Indeed by applying the magnetic criterion of aromaticity, viz. NICS(0) (see Theoretical Methods), for each of the peripheral rings, we were able to diagnose significant aromatic character, which is quantified by the NICS(0) values compiled in Table 1.

The large negative values (note that NICS of [*cyclo*-C_3H_3]$^+$ is approximately −22.4 at the same level of theory) indicate *aromatic* ring currents in all types of the peripheral three-membered rings. Obviously, the extra stabilization of the structures with peripheral aromatic rings is the outcome of the aromatic stabilization energy due to the peripheral rings. The aromatic stabilization energy based on the fully substituted *cyclo*-$Au_3(\mu\text{-L})_3$ clusters was predicted to be 17.3, 10.1, and 13.3 kcal/mol per peripheral ring for the amido-, hydroxo-, and chloro-bridged derivatives, respectively. It should be noted that the aromatic stabilization energy (ASE) of benzene is approximately 30 kcal/mol.[47]

Another interesting example of aromatic *cyclo*-$Au_3(\mu\text{-L})_3$ clusters is the [*cyclo*-$Au_3(\mu\text{-NHC})_3$]$^{3+}$, **22**, complex containing bridging N-heterocyclic-carbene (NHC) ligands.

Noteworthy is the perfectly planar configuration of high symmetry (D_{3h}) of **22** involving three peripheral isosceles Au_2C triangles, while the carbene ligands are perpendicular to the Au_3 face. The equilibrium structure of **22** resembles that of the recently[48] isolated and highly luminescent [*cyclo*-$Ag_3(\mu\text{-NHC})_3$]$^{3+}$ complex containing very short Ag−Ag separations

(47) Schleyer, P. v. R.; Puhlhofer, F. *Org. Lett.* **2002**, *4*, 2873.
(48) Catalano, V. J.; Malwitz, M. A. *Inorg. Chem.* **2003**, *42*, 5483.

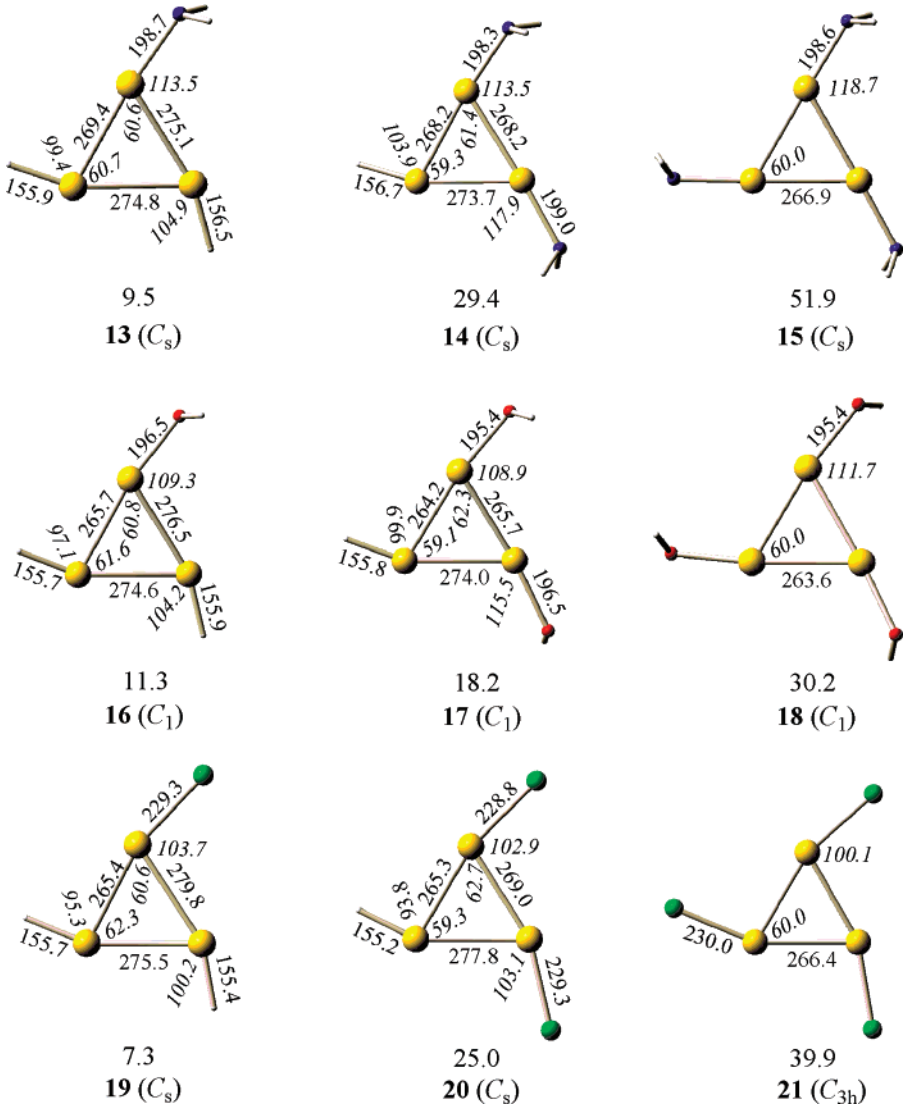

Figure 2. Equilibrium geometries (bond lengths in pm, angles in deg) and relative energies with respect to the global minima (in kcal/mol) of the *cyclo*-$Au_3L_nH_{3-n}$ (L = NH_2, OH, and Cl; n = 1, 2, 3) molecules corresponding to local minima in the PES computed at the B3LYP/LANL2DZ+*f*(Au)∪6-31G**(L) level of theory.

between 272.5 and 277.2 pm. Moreover, the Au−C bond distances of the symmetric carbene bridges compare well to those of Ag−C found in the range 222.3−226.6 pm. The negative NICS(0) values of the central Au_3 (−10.1 ppm) and the peripheral Au_2C (−15.9 ppm) rings illustrate their remarkable aromatic character. Obviously, one could think that the high stability of the $[cyclo\text{-}Ag_3(\mu\text{-}NHC)_3]^{3+}$ complex might be due to the aromaticity of the Ag_3 and Ag_2C rings.

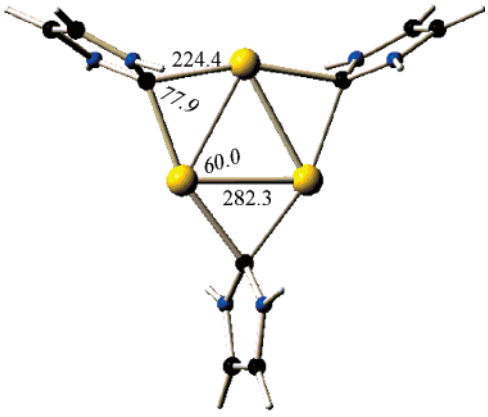

22 (D_{3h})

Table 1. NICS(0) Values (ppm) of the Au_3 and the Peripheral Rings of the *cyclo*-$Au_3(\mu\text{-L})H_2$, *cyclo*-$Au_3(\mu\text{-L})_2(\mu\text{-H})$, and *cyclo*-$Au_3(\mu\text{-L})_3$ (L = NH_2, OH, and Cl; n = 1, 2, 3) Clusters, Computed at the GIAO/B3LYP/LANL2DZ+*f*(Au)∪6-31G**(L) Level of Theory

	NICS(0)		
cluster	Au_3 ring	Au_2L ring	Au_2H ring
cyclo-$Au_3(\mu\text{-}NH_2)H_2$	−15.6	−21.1	
cyclo-$Au_3(\mu\text{-}NH_2)_2(\mu\text{-H})$	−11.5	−16.5	−28.8
cyclo-$Au_3(\mu\text{-}NH_2)_3$	−6.0	−14.2	
cyclo-$Au_3(\mu\text{-OH})H_2$	−11.0	−21.4	
cyclo-$Au_3(\mu\text{-OH})_2(\mu\text{-H})$	−12.2	−13.9	−29.3
cyclo-$Au_3(\mu\text{-OH})_3$	−7.1	−13.3	
cyclo-$Au_3(\mu\text{-Cl})H_2$	−9.8	−20.2	
cyclo-$Au_3(\mu\text{-Cl})_2(\mu\text{-H})$	−10.9	−17.5	−33.6
cyclo-$Au_3(\mu\text{-Cl})_3$	−8.9	−19.4	

Let us now discuss the most prominent structural features of the *cyclo*-$Au_3L_nH_{3-n}$ (L = CH_3, NH_2, OH, and Cl; n = 1, 2, 3) molecules. The core structure of the clusters consists of an Au_3

Table 2. Binding Energies ΔE_1 and ΔE_2 (in kcal mol^{-1}) of the *cyclo*-$Au_3L_nH_{3-n}$ (L = CH_3, NH_2, OH, and Cl; n = 1, 2, 3) Clusters Computed at the B3LYP/LANL2DZ+*f*(Au)∪6-31G**(L) Level of Theory

cluster	ΔE_1[a]	ΔE_2[b]	cluster	ΔE_1	ΔE_2
cyclo-$Au_3(CH_3)H_2$ (C_s), **1**	−30.3	−229.1	*cyclo*-$Au_3(\mu\text{-Cl})_3$ (D_{3h}), **12**	−95.0	−264.4
cyclo-$Au_3(CH_3)_2H$ (C_s), **2**	−34.4	−222.9	*cyclo*-$Au_3(NH_2)H_2$ (C_s), **13**	−36.7	−229.3
cyclo-$Au_3(CH_3)_3$ (C_{3h}), **3**	−38.1	−216.4	*cyclo*-$Au_3(NH_2)_2H$ (C_s), **14**	−48.6	−224.8
cyclo-$Au_3(\mu\text{-}NH_2)H_2$ (C_{2v}), **4**	−46.2	−238.7	*cyclo*-$Au_3(NH_2)_3$ (C_s), **15**	−62.1	−221.8
cyclo-$Au_3(\mu\text{-}NH_2)_2(\mu\text{-H})$ (C_{2v}), **5**	−78.0	−254.2	*cyclo*-$Au_3(OH)H_2$ (C_1), **16**	−38.6	−241.6
cyclo-$Au_3(\mu\text{-}NH_2)_3(D_{3h})$, **6**	−114.1	−273.7	*cyclo*-$Au_3(OH)_2H$ (C_1), **17**	−51.6	−248.6
cyclo-$Au_3(\mu\text{-OH})H_2$ (C_s), **7**	−49.9	−252.9	*cyclo*-$Au_3(OH)_3$ (C_1), **18**	−65.4	−256.4
cyclo-$Au_3(\mu\text{-OH})_2(\mu\text{-H})$ (C_s), **8**	−69.8	−266.8	*cyclo*-$Au_3(Cl)H_2$ (C_s), **19**	−38.1	−233.9
cyclo-$Au_3(\mu\text{-OH})_3$ (C_{3v}), **9**	−94.9	−286.0	*cyclo*-$Au_3(Cl)_2H$ (C_s), **20**	−41.7	−230.6
cyclo-$Au_3(\mu\text{-Cl})H_2$ (C_s), **10**	−45.4	−241.2	*cyclo*-$Au_3(Cl)_3$ (C_{3h}), **21**	−55.2	−224.6
cyclo-$Au_3(\mu\text{-Cl})_2(\mu\text{-H})$ (C_s), **11**	−73.0	−255.5	*cyclo*-$Au_3(NHC)_3$ (D_{3h}), **22**	−127.7	−324.4

[a] $\Delta E_1 = E(Au_3L_nH_{3-n}) - [nE(AuL) + (3-n)E(AuH)]$. [b] $\Delta E_2 = E(Au_3L_nH_{3-n}) - [3E(Au) + nE(L) + (n-3)E(H)]$.

triangle either isosceles or equilateral depending on the degree of substitution. The computed Au−Au separation distances in the *cyclo*-$Au_3L_nH_{3-n}$ molecules, except the *cyclo*-$Au_3(\mu\text{-L})H_2$ (L = NH_2, OH, or Cl) species, found in the range 263.6−304.3 pm are shorter than the sum of the van der Waals radii, thus strongly suggesting the existence of strong closed-shell Au···Au interactions. For the *cyclo*-$Au_3(\mu\text{-L})H_2$ (L = NH_2, OH, or Cl) species, the Au−Au separation distance participating in the formation of the peripheral Au_2L triangle is much longer, amounting to 332.3, 337.1, and 351.6 pm for the amido-, hydroxo-, and chloro-bridged derivatives, respectively. For such Au···Au separation distances, aurophilic interactions should be very weak. Interestingly, upon formation of the peripheral triangles the central Au_3 triangle is expanded: compare for example the Au−Au distances of the equilateral triangles of the fully substituted derivatives (266.9 vs 293.0 pm for *cyclo*-$Au_3(NH_2)_3$, 263.6 vs 289.5 pm for *cyclo*-$Au_3(OH)_3$, and 266.4 vs 304.3 pm for *cyclo*-Au_3Cl_3). This expansion of the triangle could be attributed to the electron delocalization over the peripheral aromatic rings as well.

The computed Au−CH_3, Au−NH_2, Au−OH, and Au−Cl bond lengths of the terminal ligands were found to be around 205.0, 198.5, 195.4, and 228.9 pm, respectively. The Au−CH_3, Au−NH_2, Au−OH, and Au−Cl bond lengths of the $AuCH_3$, $AuNH_2$, AuOH, and AuCl monomers computed at the same level of theory predicted to be 203.2, 200.2, 195.9, and 228.7 pm, respectively, are in excellent agreement with the previously reported values.[49−52] Thus, the experimental value[50] of the Au−Cl bond length in the AuCl monomer is 219.9 pm, while the calculated value at the CCSD(T) level of theory employing different basis sets[51] was found in the range 219.9−223.0 pm. Moreover, the Au−OH bond length of 195.9 pm in the AuOH monomer matches well that of 196.3 pm computed at the more sophisticated relativistic DK3-CCSD(T) level of theory.[52] The same holds also true for the computed D_0(Au−CH_3), D_0(Au−NH_2), D_0(Au−OH), and D_0(Au−Cl) bond dissociation energies of 2.57, 2.31, 2.76, and 2.45 eV, respectively. The experimental value of D_0(Au−CH_3), determined by ion cyclotron resonance experiments at 0 K, was found to be 2.15 ± 0.16 eV,[53] while the D_0(Au−Cl) value was found to be 3.12/2.86 ± 0.13 eV.[54] On the other hand, the predicted D_0(Au−OH) and D_0(Au−Cl) values of 2.76 and 2.45 eV are in excellent agreement with the D_e(Au−OH) and D_o(Au−Cl) values of 2.39 and 2.55 eV computed at the more sophisticated DK3-CCSD(T) and CCSD(T) levels of theory, respectively.[51,53] The accuracy and reliability of the computed Au−L bond lengths and dissociation energies strongly recommend the combination of the B3LYP approach with the selected basis sets to adequately describe the structural, energetic, spectroscopic, and electronic properties of the *cyclo*-$Au_3L_nH_{3-n}$ (L = CH_3, NH_2, OH, and Cl; n = 1, 2, 3) molecules, which are characterized by the closed-shell d^{10}−d^{10} intermetallic interactions.

Stability of the *cyclo*-$Au_3L_nH_{3-n}$ (L = CH_3, NH_2, OH, and Cl; n = 1, 2, 3) Molecules. The stability of the *cyclo*-$Au_3L_nH_{3-n}$ (L = CH_3, NH_2, OH and Cl; n = 1, 2, 3) molecules are investigated using the following fragmentation schemes:

$$\textit{cyclo}\text{-}Au_3L_nH_{3-n} \rightarrow n\text{AuL} + (3-n)\text{AuH}$$

$$\textit{cyclo}\text{-}Au_3L_nH_{3-n} \rightarrow 3\text{Au} + n\text{L} + (3-n)\text{H}$$

The calculated binding energies are compiled in Table 2.

It can be seen that all *cyclo*-$Au_3L_nH_{3-n}$ molecules are predicted to be bound with respect to their dissociation to either the AuL and/or AuH monomers or to free M, L, and H moieties in their ground states. Noteworthy is the increase of stabilization upon increasing substitution, being more pronounced in the aromatic gold(I) triangles surrounded by peripheral rings.

We have also computed the heat of formation of the *cyclo*-Au_3L_3 species from Au(g) and L_2(g) according to the chemical equation:

$$3\text{Au(g)} + (^3/_2)\text{L−L} \rightarrow \textit{cyclo}\text{-}Au_3L_3$$

It was found that all formation processes of the *cyclo*-$Au_3(\mu\text{-L})_3$ and *cyclo*-Au_3L_3 molecules are exothermic indicating that these species could be formed in MS of gold vapor sputtered with ethane, hydrazine, hydrogen peroxide, and chlorine or by the normal spectroscopic approach of deposition of the metal in an ethane, hydrazine, hydrogen peroxide, and chlorine matrix. The computed exothermicities for the *cyclo*-$Au_3(\mu\text{-}NH_2)_3$, *cyclo*-$Au_3(\mu\text{-OH})_3$, and *cyclo*-$Au_3(\mu\text{-Cl})_3$ clusters were found to be −184.0, −214.3, and −194.3 kcal/mol, respectively. On the other hand, the exothermicities of the formation reactions of the *cyclo*-$Au_3(CH_3)_3$, *cyclo*-$Au_3(NH_2)_3$, *cyclo*-$Au_3(OH)_3$, and *cyclo*-Au_3Cl_3 isomers were predicted to be −87.0, −132.1,

(49) Hoz, T.; Basch, H. In *The chemistry of organic derivatives of gold and silver*; Patai, S., Rappoport, Z., Eds.; John Wiley & Sons: Chichester, 1999; p 1.
(50) Evans, C. J.; Gerry, M. C. L. *J. Mol. Spectrosc.* **2000**, *203*, 105.
(51) Puzzarini, C.; Peterson, K. A. *Chem. Phys.* **2005**, *311*, 177.
(52) Ikeda, S.; Nakajima, T.; Hirao, K. *Mol. Phys.* **2003**, *101*, 105.
(53) Chowdury, A. K.; Wilkins, C. L. *J. Am. Chem. Soc.* **1987**, *109*, 5336.
(54) Brown, J. R.; Schwerdtfeger, P.; Schröder, D.; Schwarz, H. *J. Am. Soc. Mass Spectrom.* **2002**, *13*, 485.

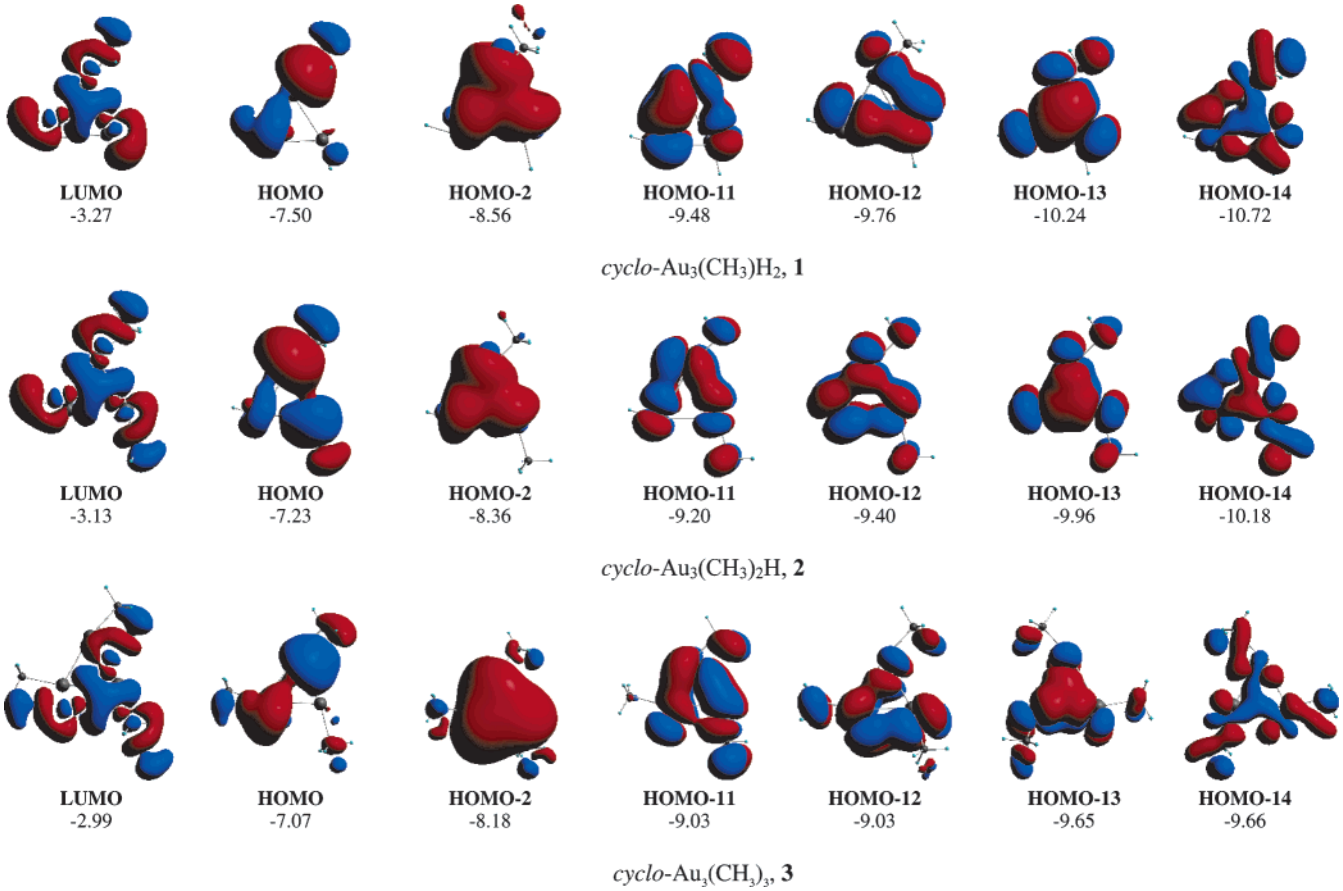

Figure 3. Most relevant valence molecular orbitals of the *cyclo*-$Au_3(CH_3)_nH_{3-n}$ ($n = 1, 2, 3$) compounds (isocontour value of 0.01 au; eigenvalues in eV).

184.7, and −154.5 kcal/mol, respectively. It is worth noting that the formation of the monomeric AuL(g) species by reacting Au(g) and L_2(g) according to the reaction

$$2Au(g) + L_2(g) \rightarrow 2AuL(g)$$

are also exothermic processes, the computed exothermicities being −32.5, −46.6, −79.5, and −66.2 kcal/mol, for the $AuCH_3$(g), $AuNH_2$(g), AuOH(g), and AuCl(g), respectively.

To understand deeper the planarity and structural integrity of the *cyclo*-$Au_3L_nH_{3-n}$ (L = CH_3, NH_2, OH, and Cl; $n = 1, 2, 3$) molecules, the most relevant valence molecular orbitals and the electronic and bonding properties have been analyzed.

Electronic and Bonding Properties of the *cyclo*-$Au_3L_nH_{3-n}$ (L = CH_3, NH_2, OH, and Cl; $n = 1, 2, 3$) Molecules. The most relevant valence molecular orbitals of selected *cyclo*-$Au_3L_nH_{3-n}$ (L = CH_3, NH_2, OH, and Cl; $n = 1, 2, 3$) molecules are shown in Figures 3 and 4.

Perusal of Figures 3 and 4 reveals that all three-membered gold(I) rings exhibit a composite bonding mode involving both σ, π and δ components. Noteworthy is the presence of highly delocalized π- and δ-type MOs, such as the HOMO-2 (δ-MO), HOMO-11, HOMO-12, and HOMO-13 (π-MOs) for the three-membered rings (Figure 3), resulting from the bonding interaction of the 5d AOs of the ring Au(I) atoms similar to the π-type MOs ($p_\pi - p_\pi$ overlap) of the corresponding substituted derivatives of the cyclopropenium cation and the bora-cyclopropene carbacyclic analogues (the most relevant MOs are shown in Figure S1), which support a ring current. The δ-MO ($d_\delta - d_\delta$ overlap) of the *cyclo*-$Au_3(\mu\text{-}NH_2)H_2$ cluster corresponds to HOMO-7 and to HOMO-9 for the *cyclo*-$Au_3(\mu\text{-}NH_2)_2H$ and *cyclo*-$Au_3(\mu\text{-}NH_2)_3$ molecules. The π-MOs ($d_\pi - d_\pi$ overlap) are the HOMO-12 and HOMO-13 for *cyclo*-$Au_3(\mu\text{-}NH_2)H_2$ and *cyclo*-$Au_3(\mu\text{-}NH_2)_2H$ clusters and HOMO-14 for *cyclo*-$Au_3(\mu\text{-}NH_2)_3$. Moreover, there exist also highly delocalized σ-type MOs ($d_\sigma - d_\sigma$ overlap) such as the HOMO-16, HOMO-15, and HOMO-15 for **4**, **5**, and **6** clusters, respectively (Figure 4). The delocalized σ and π electron density in the rings could be associated with the cyclic delocalization of electron density, which is a characteristic feature of aromaticity. Interestingly, in the peripheral three-membered rings there are both σ- and π-type MOs (HOMO-16, HOMO-18, and HOMO-19) resulting from the bonding combination of the 5d AOs of Au(I) atoms of the rings with the 1s and *n*p AOs of the H and L bridges, respectively. These MOs contribute to the cyclic delocalization of σ- and π-electron density which introduces a diatropic ring current characteristic of aromaticity of the rings, as it was corroborated by the computed NICS(0) values. Generally, the electronic structure and bonding properties of the three-membered gold(I) rings closely resemble those of the aromatic *cyclo*-$[Hg_3]^{4-}$ tetraanion, an important building block studied in the solid state in great detail, suggested as an analogue to Au_3 rings by one of the referees.

Selected electronic parameters of the *cyclo*-$Au_3L_nH_{3-n}$ (L = CH_3, NH_2, OH, and Cl; $n = 1, 2, 3$) clusters have been collected in Table 3.

Considering the inability of conventional Kohn−Sham methods (LDA and GGA) to properly treat bound and stable anions

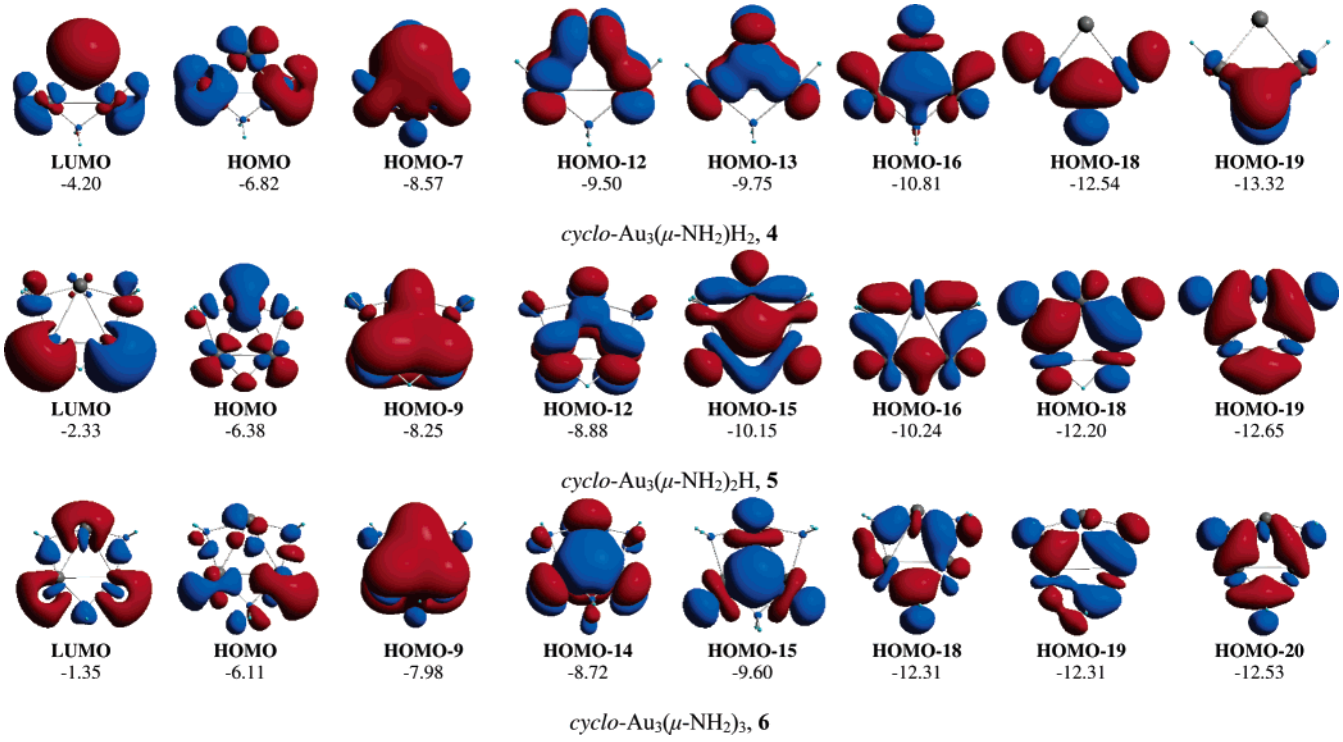

Figure 4. Most relevant valence molecular orbitals of the *cyclo*-$Au_3(\mu\text{-}NH_2)H_2$, *cyclo*-$Au_3(\mu\text{-}NH_2)_2H$, and *cyclo*-$Au_3(\mu\text{-}NH_2)_3$ molecules (isocontour value of 0.01 au; eigenvalues in eV).

Table 3. Selected Electronic Parameters of the *cyclo*-$Au_3L_nH_{3-n}$ (L = CH_3, NH_2, OH, and Cl; n = 1, 2, 3) Clusters Computed at the B3LYP/LANL2DZ+*f*(Au)∪6-31G**(L) Level of Theory

					5d/6s		q_M[b]	
compound	ϵ_{HOMO}	ϵ_{LUMO}	η	ω[a]	Au(1)	Au(2); Au(3)	Au(1)	Au(2); Au(3)
1	−7.50	−3.27	2.12	3.42	9.68/1.04	9.76/1.11	0.27	0.12
2	−7.23	−3.13	2.05	3.27	9.68/1.05	9.76/1.11	0.26	0.11
3	−7.07	−2.99	2.04	3.10	9.68/1.05		0.26	
4	−6.81	−4.20	1.31	5.76	9.97/0.62	9.68/0.95	0.37	0.36
5	−6.38	−2.33	2.03	2.34	9.67/081	9.82/0.72	0.51	0.44
6	−6.11	−1.35	2.38	1.46	9.68/0.85		0.49	
7	−7.00	−4.37	1.32	6.13	9.97/0.64	9.67/0.95	0.35	0.37
8	−6.85	−3.28	1.78	3.59	9.67/0.73	9.84/0.63	0.58	0.50
9	−6.81	−2.76	2.02	2.83	9.69/0.69		0.59	
10	−7.31	−4.50	1.40	6.21	9.97/0.62	9.73/0.93	0.38	0.31
11	−7.69	−3.52	2.08	3.77	9.82/0.65	9.86/0.66	0.50	0.45
12	−7.88	−3.05	2.42	3.09	9.82/0.66		0.50	
13	−7.04	−3.62	1.71	4.16	9.63/0.94	9.74/1.08	0.39	0.16; 0.09
14	−6.81	−3.80	1.50	4.68	9.60/0.94	9.73/1.11	0.43	0.34; 0.13
15	−6.79	−3.94	1.42	5.06	9.68/0.82	0.49		
16	−7.48	−3.96	1.76	4.87	9.61/0.89	9.76/1.11	0.45	0.19; 0.11
17	−7.59	−4.50	1.54	5.91	9.56/0.89	9.71/1.08	0.51	0.42; 0.18
18	−7.95	−5.04	1.45	7.27	9.54/0.92		0.49	
19	−7.83	−4.27	1.78	5.13	9.75/0.83	9.76/1.08	0.37	0.20; 0.14
20	−8.15	−5.08	1.53	7.12	9.70/0.84	9.71/1.03	0.41	0.39; 0.23
21	−8.62	−5.84	1.39	9.41	9.69/0.83		0.44	
22	−16.41	−12.64	1.88	28.00	9.76/0.69		0.54	

[a] Electrophilicity index $\omega = \mu^2/2\eta$, where μ and η are the chemical potential and hardness, respectively, given approximately by the expressions $\mu = (\epsilon_{LUMO} + \epsilon_{HOMO})/2$ and $\eta = (\epsilon_{LUMO} - \epsilon_{HOMO})$. ϵ_{HOMO}, ϵ_{LUMO}, η, and ω are given in eV. [b] Natural atomic charges.

of small or medium size, we calculated the molecular and electronic structure of *cyclo*-$[Hg_3]^{4-}$ at the MP2/LANL2DZ. The equilibrium structure corresponds to an isosceles triangle (D_{3h} point group) with Hg−Hg bond lengths of 309.8 pm, which are much shorter than the sum of the van der Waals radii (352.0 pm).[1] The most relevant valence MOs of the *cyclo*-$[Hg_3]^{4-}$ tetraanion are shown in Scheme 1.

One can easily see the analogous pattern of the MOs of the three-membered gold(I) rings and the *cyclo*-$[Hg_3]^{4-}$ analogue.

The high stability of the *cyclo*-$Au_3L_nH_{3-n}$ (L = CH_3, NH_2, OH, and Cl; n = 1, 2, 3) rings is also reflected on the high $\epsilon_{LUMO} - \epsilon_{HOMO}$ energy gap, the so-called global hardness η. According to the computed η values the stability of the *cyclo*-$Au_3(\mu\text{-}L)_3H_{3-n}$ clusters increases upon increasing the degree of substitution, which is consistent with the increase of the aromatic stabilization energy due to the increase of the number of the peripheral aromatic rings. However, the opposite is true for the *cyclo*-$Au_3L_3H_{3-n}$ clusters involving terminal L groups.

Scheme 1

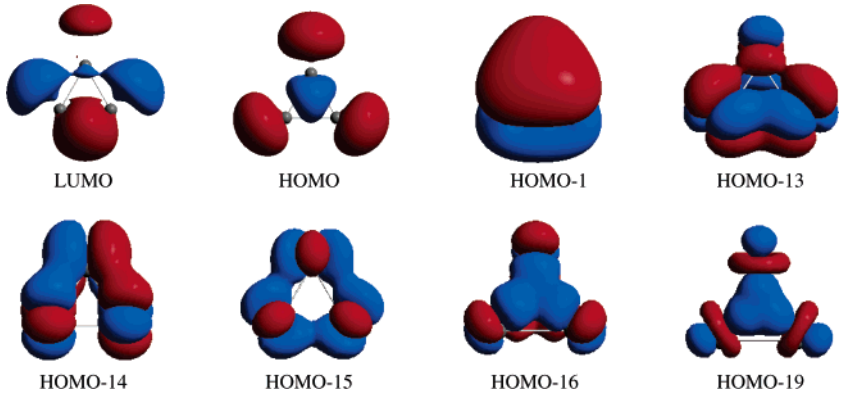

Table 4. ^{1}H, ^{13}C, ^{14}N, ^{17}O, ^{35}Cl, and ^{197}Au Isotropic Shielding Tensor Elements (σ^{iso}, ppm) and the NICS(0) Values (ppm) for the *cyclo*-$Au_3L_nH_{3-n}$ (L = CH_3, NH_2, OH, and Cl; n = 1, 2, 3), Computed at the GIAO/B3LYP/LANL2DZ+*f*(Au)∪6-31G**(L) Level of Theory

	σ^{iso}						
cluster	^{1}H	^{13}C	^{14}N	^{17}O	^{35}Cl	^{197}Au	NICS(0)
cyclo-$Au_3(CH_3)H_2$, **1**	31.2	172.6				219.6 (203.8)	−17.5 (−22.9)[a]
cyclo-$Au_3(CH_3)_2H$, **2**	31.2	171.1				218.5 (203.7)	−18.0 (−23.3)
cyclo-$Au_3(CH_3)_3$, **3**		169.9				203.7	−18.5 (−23.5)
cyclo-$Au_3(\mu\text{-}NH_2)H_2$, **4**	33.6		243.0			252.7 (187.1)	−15.6
cyclo-$Au_3(\mu\text{-}NH_2)_2(\mu\text{-}H)$, **5**	32.3		262.3			204.4 (161.3)	−11.5
cyclo-$Au_3(\mu\text{-}NH_2)_3$, **6**			306.5			153.6	−6.0
cyclo-$Au_3(\mu\text{-}OH)H_2$, **7**	35.3			307.5		254.7 (176.7)	−11.0
cyclo-$Au_3(\mu\text{-}OH)_2(\mu\text{-}H)$, **8**	32.7			371.0		208.1 (132.7)	−12.2
cyclo-$Au_3(\mu\text{-}OH)_3$, **9**				472.4		118.7	−7.1
cyclo-$Au_3(\mu\text{-}Cl)H_2$, **10**	33.1				75.9	251.2 (196.6)	−9.8
cyclo-$Au_3(\mu\text{-}Cl)_2H$, **11**	32.4				77.1	214.6 (193.0)	−10.9
cyclo-$Au_3(\mu\text{-}Cl)_3$, **12**					86.9	175.4	−8.9
cyclo-$Au_3(NH_2)H_2$, **13**	31.2		213.0			217.6 (180.0)	−19.3 (−27.0)
cyclo-$Au_3(NH_2)_2H$, **14**	30.8		194.6			215.9 (181.4)	−21.3 (−31.6)
cyclo-$Au_3(NH_2)_3$, **15**			175.3			182.8	−26.1 (−35.1)
cyclo-$Au_3(OH)H_2$, **16**	31.4			272.7		216.5 (182.1)	−19.8 (−25.8)
cyclo-$Au_3(OH)_2H$, **17**	31.4			225.6		211.7 (162.0)	−23.6 (−29.9)
cyclo-$Au_3(OH)_3$, **18**				170.5		156.7	−27.7 (−33.8)
cyclo-$Au_3(Cl)H_2$, **19**	31.6				65.4	213.6 (204.8)	−19.0 (−23.1)
cyclo-$Au_3(Cl)_2H$, **20**	31.8				58.1	206.4 (202.1)	−21.5 (−23.8)
cyclo-$Au_3(Cl)_3$, **21**					49.3	196.8	−23.8 (−24.4)
cyclo-$Au_3(NHC)_3$, **22**		62.9				192.0	−10.1

[a] Figures in parentheses are the NICS(0) values of the corresponding substituted derivatives of cyclopropenium cation computed at the GIAO/B3LYP/6-31G(d,p) level of theory.

The extent of aromaticity of the *cyclo*-$Au_3L_nH_{3-n}$ (L = CH_3, NH_2, OH, and Cl; n = 1, 2, 3) clusters is also mirrored on the computed[55] electrophilicity index $\omega = \mu^2/2\eta$, where μ and η are the chemical potential and hardness, respectively, given approximately by the expressions $\mu = (\epsilon_{LUMO} + \epsilon_{HOMO})/2$ and $\eta = (\epsilon_{LUMO} - \epsilon_{HOMO})$. The η values also indicate that the *cyclo*-$Au_3L_nH_{3-n}$ molecules are relatively hard nucleophiles, which can readily interact with electrophiles, such as H^+, Li^+, Ag^+, and Tl^+ cations, as it was observed experimentally.[19] It is evident then why the Ag^+ and Tl^+ cations are easily stacked on the Au_3 triangle containing molecules, forming also sandwichlike complexes.[19] The structural, energetic, and electronic properties of these novel sandwichlike complexes will be discussed later on.

According to the natural bond orbital (NBO) population analysis (Table 3) there is a significant charge transfer of approximately 0.41−0.89 |e| of natural charge from the L and H ligands to Au(I) metal atoms. The charge transfer from the terminal ligands is much higher than that from the bridging ones. The transferred electronic density is accumulated on the vacant *n*s orbitals of the Au(I) having the $5d^{10}$ electron configuration. Moreover, the natural electron configurations (Table 3) indicate that there is also promotion of a relatively small amount of electron density from the $5d^{10}$ to 6s orbitals amounting to 0.03−0.46 |e|. The magnitude of the 5d → 6s electron promotion in the partially substituted derivatives depends on the position of the substituents in the three-membered gold(I) rings.

NMR Spectra and Aromaticity of the *cyclo*-$Au_3L_nH_{3-n}$ (L = CH_3, NH_2, OH, and Cl; n = 1, 2, 3) Clusters. Planarity, high stability, bond length equalization, and hardness are conventionally good indicators of aromaticity, but this is restrictive in many examples. To verify further the aromaticity of the *cyclo*-$Au_3L_nH_{3-n}$ (L = CH_3, NH_2, OH, and Cl; n = 1, 2, 3) molecules, the absolute ^{1}H, ^{13}C, ^{14}N, ^{17}O, ^{35}Cl, and ^{197}Au isotropic shielding tensor elements (σ^{iso} ppm) were calculated at the GIAO/B3LYP/LANL2DZ+*f*(Au)∪6-31G**(L) level of theory. The absolute isotropic shielding tensor elements are compiled in Table 4. Notice that the computed NMR spectra of the *cyclo*-$Au_3L_nH_{3-n}$ (L = CH_3, NH_2, OH, and Cl; n = 1, 2, 3) compounds are predictions as there are no experimental data

(55) Parr, R. G.; v. Szentpaly, L.; Liu, S. *J. Am. Chem. Soc.* **1999**, *121*, 1922.

Scheme 2

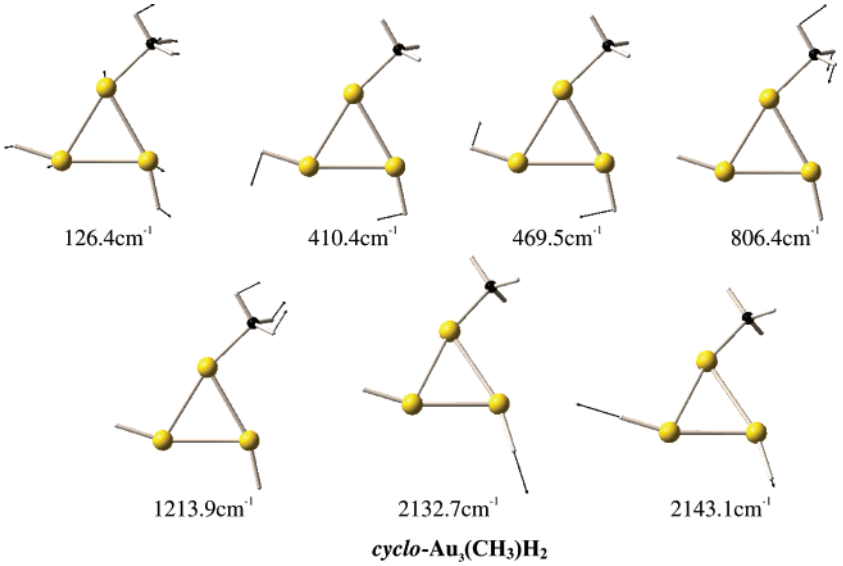

available so far and therefore could assist experimentalists in identifying the respective compounds. Moreover, to quantify further the aromaticity/antiaromaticity of the three-membered gold(I) rings we computed the NICS(0) values which are also given in Table 4.

It can be seen that all *cyclo*-$Au_3L_nH_{3-n}$ (L = CH_3, NH_2, OH and Cl; n = 1, 2, 3) molecules exhibit negative NICS(0) values, the absolute values increasing as the degree of substitution increases. It seems that NICS(0) depends on the ring size, following the reverse trend of the triangular gold(I) ring area. Moreover, the increase of the aromatic character as the degree of substitution increases is also mirrored on the deshielding (downfield chemical shifts) of the ^{13}C, ^{14}N, ^{17}O, ^{35}Cl, and ^{197}Au shielding tensor elements. Noteworthy is the higher aromatic character of the *cyclo*-$Au_3L_nH_{3-n}$ molecules with respect to the *cyclo*-$Au_3(\mu\text{-}L)_nH_{3-n}$ isomers. Interestingly, the high NICS(0) values of the *cyclo*-$Au_3L_nH_{3-n}$ molecules (ranging from −17.5 to −27.7 ppm) are comparable to the NICS(0) values of the corresponding aromatic substituted derivatives of cyclopropenium cation (ranging from −22.9 to −35.1 ppm). Moreover, the NICS(0) values of the neutral *cyclo*-$C_2B_nR_3$ (R = Me, NH_2, OH, and Cl) bora-cyclopropene carbacyclics found to be −21.2, −32.1, −33.3, and −24.0 ppm for the methyl-, amino-, hydroxy-, and chloro-derivatives, respectively, compare also well with those of the corresponding *cyclo*-Au_3R_3 molecules. It should also be noted that the extent of diatropicity of the *cyclo*-$Au_3L_nH_{3-n}$ molecules, measured by the NICS(0) values, is comparable to that of the *cyclo*-$[Hg_3]^{4-}$ analogue (NICS(0) = 18.0 ppm at the MP2/LANL2DZ level) as well as to that of the three-membered Ga_3 ring (NICS(0) = −17.6 ppm), which constitutes the core structure in $M_2[(2,6\text{-}Mes_2C_6H_3)Ga]_3$ (M = Li, Na, K; Mes = 2,4,6-$Me_3C_6H_2$-) compounds.[56] In the presence of the M^+ cations, which are associated with the *cyclo*-$[(GaH)_3]^{2-}$ dianion along the C_3 axis, the NICS(0) values become −13, −15, and −15 ppm for Li^+, Na^+, and K^+, respectively. These findings nicely explain why the Au_3 triangles are the more common cores in the structures of polynuclear gold(I) clusters studied so far.

(56) Xi, Y.; Schreiner, P. R.; Schaefer, H. F., III; Li, X.-W.; Robinson, G. H. *J. Am. Chem. Soc.* **1996**, *118*, 10635.

Vibrational Spectra of the *cyclo*-$Au_3L_nH_{3-n}$ (L = CH_3, NH_2, OH, and Cl; n = 1, 2, 3) Clusters. The most characteristic infrared active vibrational modes of representative *cyclo*-$Au_3L_nH_{3-n}$ (L = CH_3, NH_2, OH, and Cl; n = 1, 2, 3) along with the normal coordinate vectors (arrows) are shown in Schemes 2−4. The unscaled harmonic vibrational frequencies and the IR intensities computed at the B3LYP/LANL2DZ+*f*(Au)∪6-31G**(L) level of theory are listed in detail in the Supporting Information (Tables S1 and S2).

Generally the vibrational modes of the *cyclo*-$Au_3L_nH_{3-n}$ (L = CH_3, NH_2, OH and Cl; n = 1, 2, 3) molecules resemble those of the corresponding substituted derivatives of cyclopropenium cation and the neutral bora-cyclopropene carbacyclic analogues, and the corresponding infrared absorption bands could assist in identifying the respective three-membered gold(I) rings. Despite the characteristic bands related to the vibrations of the substituents either terminal or bridging, the bands associated with the three-membered gold(I) rings are of particular importance for the identification processes. These bands absorbing in the region 44−160 cm^{-1} correspond to the symmetric breathing mode and the deformation modes of the Au_3 rings. Thus, the symmetric breathing modes of the rings absorb around 126 cm^{-1}, 135−152 cm^{-1}, 139−160 cm^{-1}, and 137−143 cm^{-1} for the methyl-, amido-, hydroxo-, and chloro-substituted derivatives. In general terms the symmetric breathing vibrational modes are shifted to higher frequencies as the degree of substitution increases. All aromatic Au_3 rings show two ring deformation vibrational modes absorbing in the region 44−137 cm^{-1}. These bands are found at lower frequencies with respect to the symmetric breathing vibrational modes in all Au_3 rings studied, following the same trend for both the terminally or bridged derivatives.

Interaction of the *cyclo*-$Au_3L_nH_{3-n}$ (L = CH_3, NH_2, OH, and Cl; n = 1, 2, 3) Clusters with Electrophiles. To verify further the aromaticity of the *cyclo*-$Au_3L_nH_{3-n}$ (L = CH_3, NH_2, OH, and Cl; n = 1, 2, 3) clusters we also investigated the interaction of representative aromatic *cyclo*-$Au_3L_nH_{3-n}$ molecules with electrophiles. In particular, we studied the interaction of the *cyclo*-$Au_3(CH_3)_3$ and *cyclo*-$Au_3(\mu\text{-}NH_2)_3$ aromatics with Li^+ and Tl^+ ions in 1:1 and 2:1 molar ratios. We have also

Scheme 3

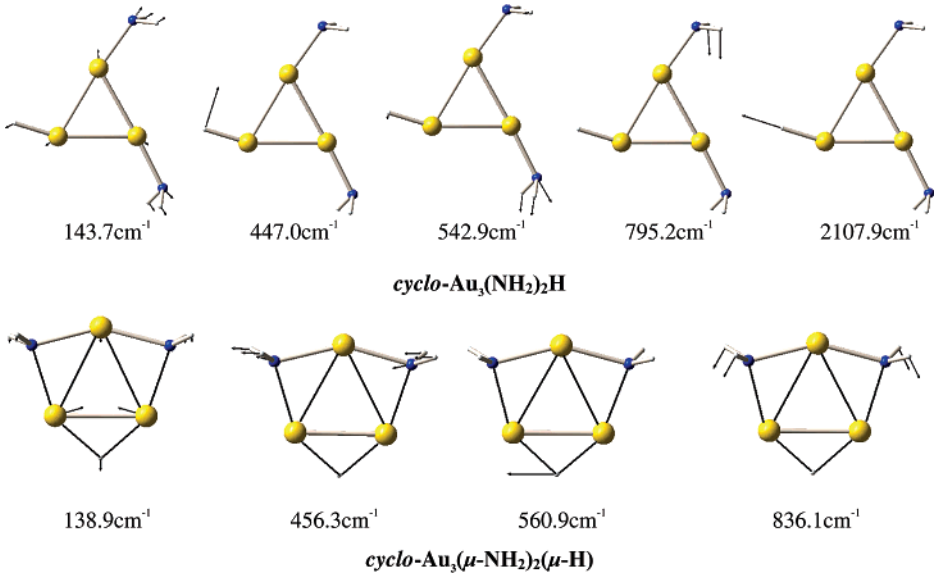

Scheme 4

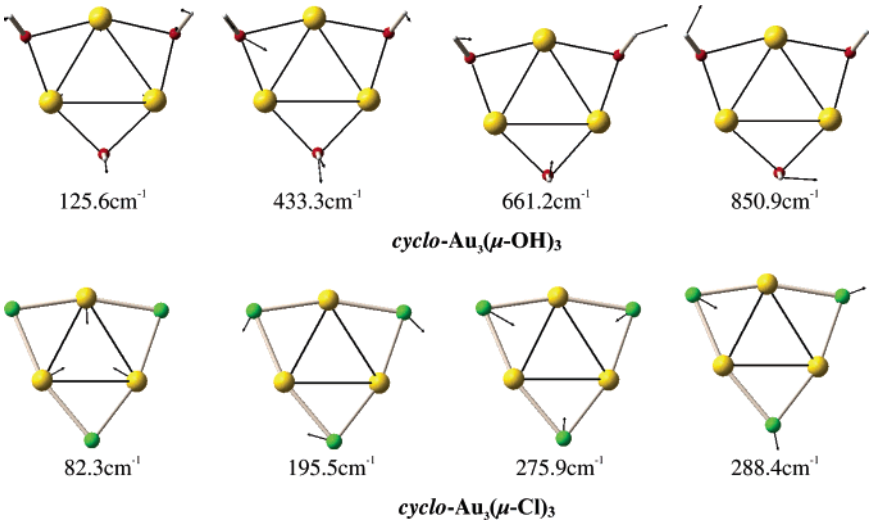

studied the interaction of the *cyclo*-$Au_3(CH_3)_3$ cluster with the H^+ electrophile, as well as with Ag^+ cations to form the 1:1 and 2:1 sandwichlike $[\{cyclo\text{-}Au_3(CH_3)_3\}_2Ag]^+$ complexes. These electrophiles have been selected on the basis of the well-known tendency of triangular gold(I) clusters to interact with such metal cations to form sandwichlike complexes.[19,57] The equilibrium structures of the new 1:1 and 2:1 clusters are depicted schematically in Figures 5 and 6, respectively.

It can be seen that the electrophile M^+ (M = H, Li, Tl, Ag) attaches the Au_3 aromatic rings along the C_3 axis without changing their local symmetry. Thus, all $[\{cyclo\text{-}Au_3(CH_3)_3\}M]^+$ and $[\{cyclo\text{-}Au_3(\mu\text{-}NH_2)_3\}M]^+$ species adopt trigonal pyramidal structures belonging to C_3 and C_{3v} point groups, respectively. On the other hand, the sandwichlike $[\{cyclo\text{-}Au_3(CH_3)_3\}_2M]^+$ species have structures of S_6 symmetry with the two Au_3 aromatic rings adopting the staggered conformation. Interestingly, in the $[\{cyclo\text{-}Au_3(\mu\text{-}NH_2)_3\}_2Li]^+$ complex the two Au_3 aromatic rings have also a staggered conformation (D_{3d}), while in the $[\{cyclo\text{-}Au_3(\mu\text{-}NH_2)_3\}_2Tl]^+$ complex the two rings adopt an eclipsed conformation (D_{3h}). Inspection of the coordinated Au_3 aromatic rings reveals that the Au−Au bond lengths elongate upon complexation, the elongation being higher (13.5 pm) for the H^+ electrophile. The Li^+ electrophile introduces an elongation of the Au−Au bond distances of approximately 3.7 and 2.0 pm for the 1:1 and 2:1 complexes, respectively, while the Tl^+ electrophile introduces smaller Au−Au bond distance elongations amounting to 2.7 and 1.8 pm for the 1:1 and 2:1 complexes, respectively.

The small structural perturbations introduced by the complexation are indicative of weak interactions of the Li^+ and Tl^+ electrophiles with the aromatic three-membered gold(I) rings. This is also reflected on the relatively large distances of the Li^+ and Tl^+ from the ring centers found to be 210.2, 288.3, 195.0, and 277.9 pm for **25**, **26**, **27**, and **28**, respectively. These distances are larger in the corresponding 2:1 complexes, amounting to 224.7, 303.9, 208.5, and 295.3 pm for **29**, **30**, **31**, and **32**, respectively.

The H^+−(ring-centroid) distance in **23** is only 76.5 pm in line with the larger (13.5 pm) elongation of the Au−Au bond lengths introduced by complexation. The Ag^+−(ring-centroid)

(57) Burini, A.; Fackler, J. P., Jr.; Galassi, R.; Pietroni, B. R.; Staples, R. J. *Chem. Commun.* **1998**, 95.

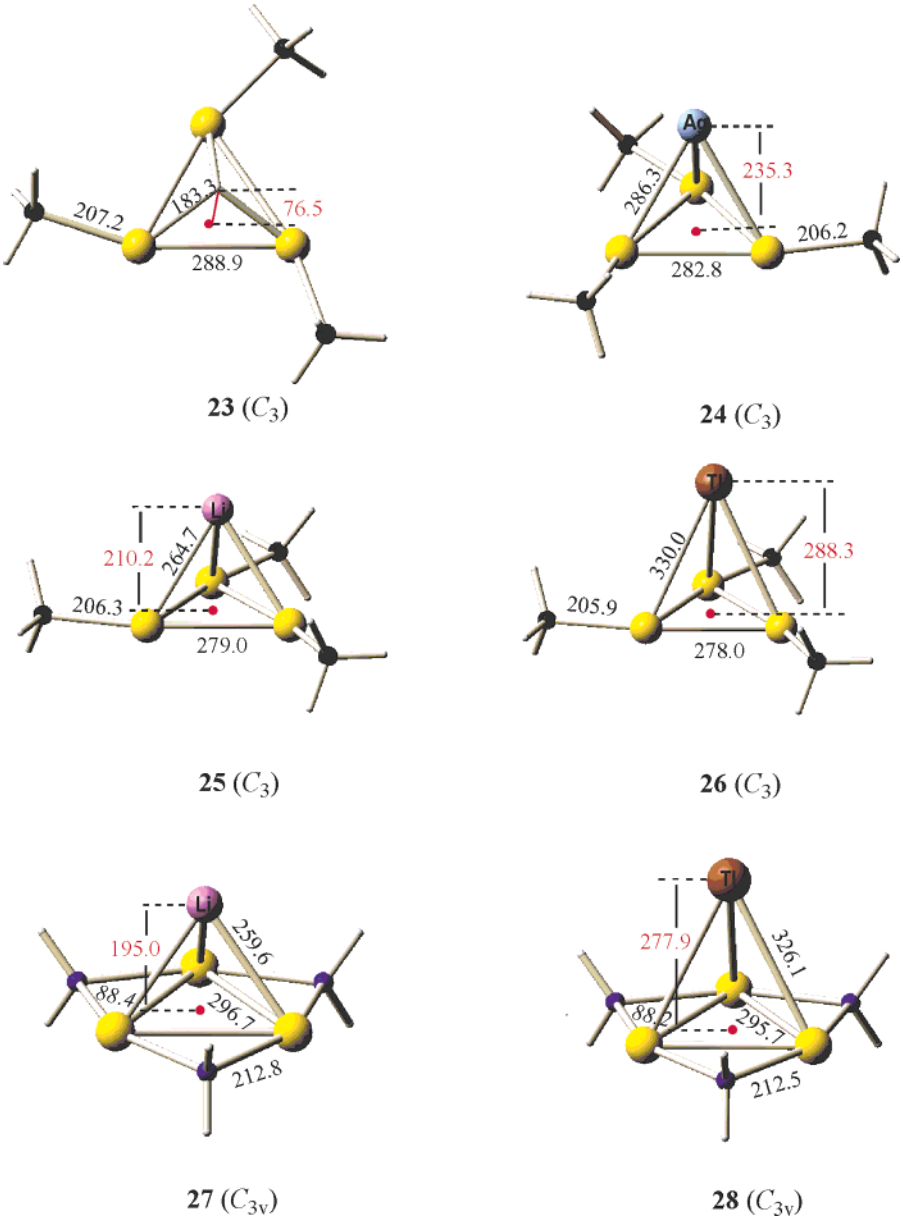

23 (C_3) **24** (C_3)

25 (C_3) **26** (C_3)

27 (C_{3v}) **28** (C_{3v})

Figure 5. Equilibrium geometries (bond lengths in pm, angles in deg) of the [{*cyclo*-$Au_3(CH_3)_3$}M]$^+$ and [{*cyclo*-$Au_3(\mu\text{-}NH_2)_3$}M]$^+$ (M = H, Ag, Li, Tl) clusters computed at the B3LYP/LANL2DZ+*f*(Au)∪6-31G**(L) level of theory.

distance in **24** is 235.3 pm illustrating stronger interactions with the aromatic Au_3 ring which is also reflected on an elongation of the Au−Au bond lengths by 7.4 pm. Generally, the M$^+$−(ring-centroid) distances increase as the M$^+$ is changed from H$^+$ to Li$^+$ to Ag$^+$ to Tl$^+$, following the increase of the ionic radii of the M$^+$. Moreover, the M$^+$−(ring-centroid) distances increase as the second aromatic Au_3 ring was added to [{*cyclo*-$Au_3(CH_3)_3$}M]$^+$ and [{*cyclo*-$Au_3(\mu\text{-}NH_2)_3$}M]$^+$ species, as expected for a bonding mechanism based primarily on electrostatic (Coulombic) interactions. However, the Au−M bond distances in the 1:1 and 2:1 complexes are shorter than the sum of the van der Waals radii of the interacting atoms (H = 120, Li = 182, Tl = 196 pm)[1], indicating that covalent interactions leading to the formation of the respective coordination bonds might also contribute to the bonding scheme. It should be noted that the Tl$^+$ cation was found to be bonded to two three-membered gold(I) rings to form a sandwichlike complex with Au−Tl distances from 297.1 to 304.5 pm in [Tl{Au(μ-N^3,C^2-bzim)$_3$}$_2$]$^+$ and from 306.7 to 310.8 in [Tl{Au(μ-C(OEt)=$NC_6H_4CH_3$)$_3$}$_2$]PF_6.[19] Moreover, the Au−Ag distances in the sandwichlike [Ag{Au(μ-N^3,C^2-bzim)$_3$}$_2$]BF_4 cluster determined by X-ray crystallography[57] range from 273.1 to 292.2 pm in excellent agreement with the computed Au−Ag bond distance 292.3 pm for the sandwichlike complex **32**.

The following hypothetical reactions can be used to assess the relative thermodynamic stabilities of the [{*cyclo*-$Au_3(L)_3$}$_2$M]$^+$ (L = CH_3, NH_2; M = H, Ag, Li, Tl) molecules:

$$[\{cyclo\text{-}Au_3(L)_3\}_2M]^+ \rightarrow [\{cyclo\text{-}Au_3(L)_3\}M]^+ + L \qquad \Delta H_1$$

$$[\{cyclo\text{-}Au_3(L)_3\}M]^+ \rightarrow L + M^+ \qquad \Delta H_2$$

The reaction enthalpies ΔH_1 and ΔH_2 for the stepwise fragmentation of the [{*cyclo*-$Au_3(L)_3$}$_2$M]$^+$ (L = CH_3, NH_2; M = H, Ag, Li, Tl) molecules computed at the GIAO/B3LYP/LANL2DZ+*f*(Au)∪6-31G**(L) level are given in Table 5.

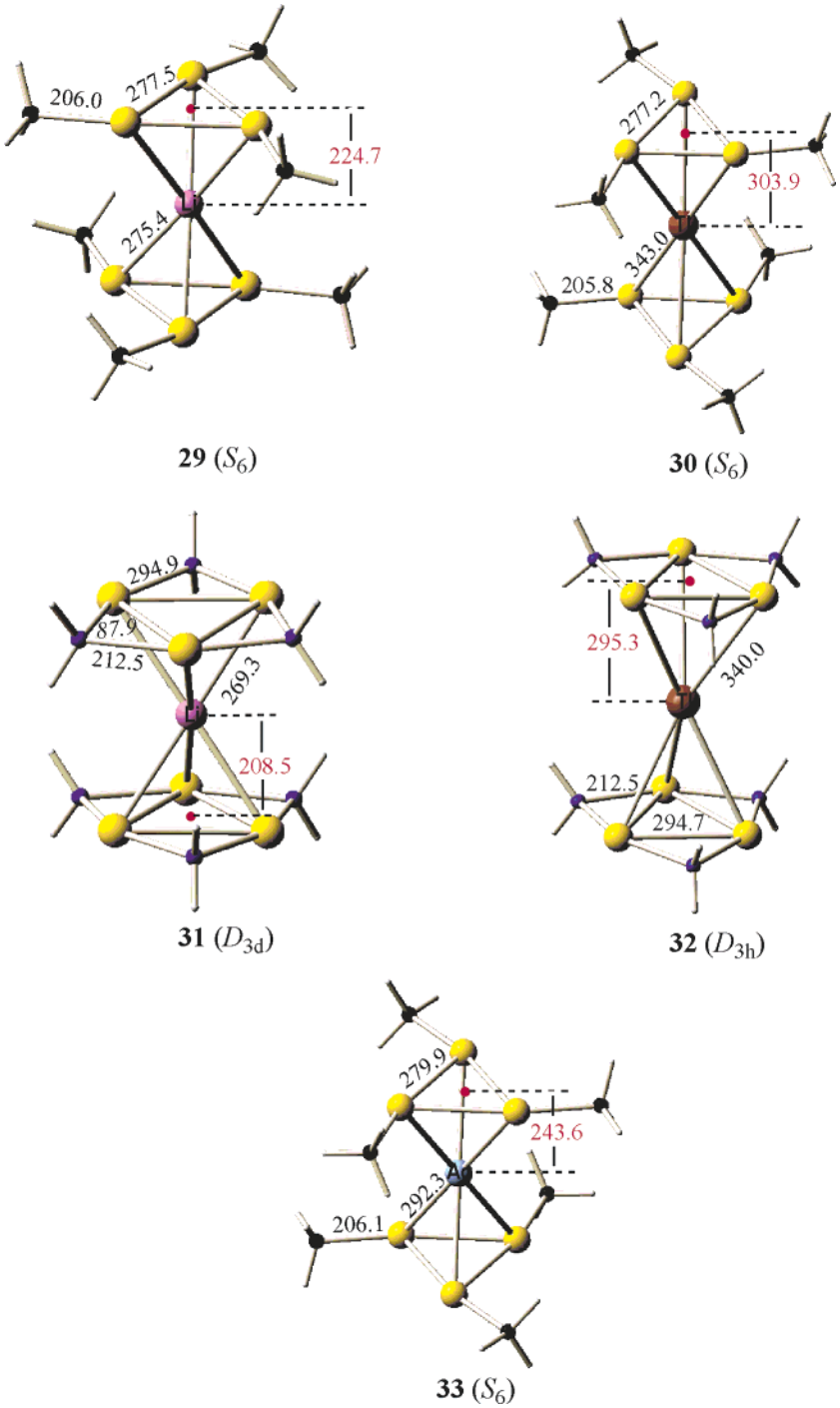

29 (S_6) **30** (S_6)

31 (D_{3d}) **32** (D_{3h})

33 (S_6)

Figure 6. Equilibrium geometries (bond lengths in pm, angles in deg) of the $[\{cyclo\text{-}Au_3(CH_3)_3\}_2M]^+$ and $[\{cyclo\text{-}Au_3(\mu\text{-}NH_2)_3\}_2M]^+$ (M = Li, Tl, Ag) clusters computed at the B3LYP/LANL2DZ+*f*(Au)∪6-31G**(L) level of theory.

Table 5. Reaction Enthalpies (kcal/mol) for the Stepwise Fragmentation of the $[\{cyclo\text{-}Au_3(L)_3\}_2M]^+$ (L = CH_3, NH_2; M = H, Ag, Li, Tl) Molecules Computed at the GIAO/B3LYP/LANL2DZ+*f*(Au)∪6-31G**(L) Level of Theory

	L = CH_3				L = NH_2	
	H	Ag	Li	Tl	Li	Tl
ΔH_1		27.4	17.4	11.0	22.4	10.8
ΔH_2	169.8	45.5	35.9	24.4	40.1	24.7

Noteworthy is the strong interaction of the proton with the aromatic Au_3 ring, the computed proton affinity being about 170 kcal/mol at the GIAO/B3LYP/LANL2DZ+*f*(Au)∪6-31G**(L) level. The next electrophile strongly interacting with the aromatic Au_3 ring is the Ag^+ ion followed by the Li^+ and Tl^+ ions. The predicted reaction enthalpy for the association of Li^+ with the aromatic Au_3 rings (35.9 and 40.1 kcal/mol) compares well with the reaction enthalpy for the association of Li^+ with the aromatic *cyclo*-Ga_3H_3 rings (about 45 kcal/mol per Li^+ computed at the B3LYP level).[56] It is also instructive to compare the $Li^+-(cyclo\text{-}Au_3L_3)$ and $(cyclo\text{-}Au_3L_3)Li^+-(cyclo\text{-}Au_3L_3)$ bond dissociation energies to those of $Li^+-C_6H_6$ and $C_6H_6Li^+-C_6H_6$ complexes (38.5 and 24.9 kcal/mol, respectively) determined experimentally by collision-induced dissociation with Xe in a guide ion beam spectrometer.[58]

Interestingly, the Li^+−(ring-centroid) distances of 210.2 and 195.0 pm in **25** and **27**, respectively, are comparable to the Li^+−(ring-centroid) distance 191.0 pm in Li^+−C_6H_6 computed at the MP2(full)/6-31G(d) level of theory. Interesting enough, the interaction of the *cyclo*-$Au_3L_nH_{3-n}$ (L = CH_3, NH_2, OH, and Cl; n = 1, 2, 3) clusters with electrophiles differs from that of the corresponding substituted derivatives of cyclopropenium cation and the neutral bora-cyclopropene carbacyclic analogues. The latter do not form half-sandwich or sandwich complexes with protons, Li^+, Ag^+, and Tl^+ electrophiles. Electrophilic attack by a proton on the cyclopropenium cation leads to ring opening or to the protonation of a C atom of the ring.[60] The neutral bora-cyclopropene carbacyclic analogues interact with a proton or Li^+ or Ag^+ forming adducts **34**, **35**, and **36**, respectively, with the electrophile bridging the two carbon atoms of the ring (η^2-C bonding). Notice that the Li^+ is coplanar with the ring plane, the H^+ is positioned slightly over the ring plane, while the Ag^+ is on the vertical line bisecting the C−C bond.

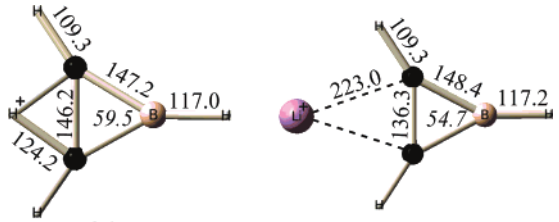

34 **35** **36**

These structures can be understood in terms of maximizing the electrostatic interactions between the electrophiles and the carbanions imbedded within the bora-cyclopropene ring. The carbon atoms in bora-cyclopropene acquires a negative natural atomic charge of −0.40 |e|, while boron bears a positive natural atomic charge of 0.36 |e|. Thus the propensity for the cations to bridge the carbon atoms results from a favorable electrostatic attraction. However, this is not the case for the *cyclo*-$Au_3L_nH_{3-n}$ (L = CH_3, NH_2, OH and Cl; n = 1, 2, 3) clusters where the gold(I) atoms acquire positive natural atomic charge, and therefore it is the delocalized π electron cloud which supports the predicted cation−π interactions.

On the other hand, the *cyclo*-$[Hg_3]^{4-}$ analogue interacts with H^+ or Li^+ exactly in the same way as the *cyclo*-$Au_3L_nH_{3-n}$ clusters affording the half-sandwich complexes **37** and **38**, respectively. It is important to note that the H^+−(ring-centroid) distance in **37** is only 37.8 pm, almost half the value of that in **23**, probably as a result of the increase of the electrostatic component of the interactions due to the excess of negative charge on the Hg_3 ring.

Finally, it should be noted that a very recent DFT study of the doubly bridged square planar coinage metal clusters, $[M_4]$-Li_2 (M = Cu, Ag and Au), disclosed distinct differences from other $[X_4]^{2-}$ systems (X = CH and Al) and provided quantitative evidence for the existence of aromaticity involving the d orbitals.[61]

Table 6. Selected Electronic Parameters[a] of the $[\{cyclo\text{-}Au_3(L)_3\}M]^+$ and $[\{cyclo\text{-}Au_3(L)_3\}_2M]^+$ (L = CH_3, NH_2; M = H, Ag, Li, Tl) Molecules Computed at the GIAO/B3LYP/LANL2DZ+*f*(Au)∪6-31G**(L) Level of Theory

					ns/*np*	5d/6s	*q*[b]	
compd	ϵ_{HOMO}	ϵ_{LUMO}	η	ω	M^+	Au	M^+	Au
23	−11.63	−8.53	1.55	16.38	1.08/0.00	9.64/0.87	−0.09	0.48
24	−11.04	−7.83	1.60	13.90	0.25/9.99[c]	9.68/1.06	0.75	0.24
25	−11.19	−7.16	2.02	10.43	0.08/0.03	9.68/1.09	0.88	0.19
26	−10.93	−6.92	2.01	9.92	1.99/0.18	9.68/1.07	0.83	0.23
27	−10.68	−5.87	2.40	7.13	0.07/0.03	9.67/0.81	0.89	0.50
28	−10.32	−5.90	2.21	7.44	1.98/0.18	9.66/0.80	0.84	0.52
29	−10.47	−6.54	1.97	9.20	0.28/0.07	9.68/1.06	0.65	0.24
30	−10.28	−6.41	1.94	8.99	1.98/0.43	9.68/1.04	0.59	0.26
31	−9.89	−5.35	2.27	6.39	0.26/0.05	9.67/0.80	0.69	0.52
32	−9.56	−5.32	2.12	6.53	1.97/0.44	9.67/0.78	0.59	0.54
33	−10.18	−6.91	1.64	11.14	0.49/9.97[a]	9.68/1.04	0.49	0.27

[a] ϵ_{HOMO}, ϵ_{LUMO}, η, and ω are given in eV. [b] Natural atomic charges. [c] 4d natural electronic configuration of Ag.

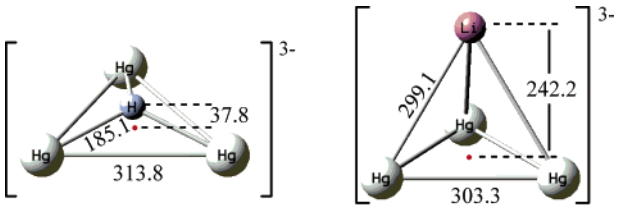

37 **38**

To gain insight into the electronic structure and the bonding mechanism of the $[\{cyclo\text{-}Au_3(L)_3\}_2M]^+$ and $[\{cyclo\text{-}Au_3(L)_3\}M]^+$ complexes we analyzed their molecular orbitals (Figure 7), while selected electronic parameters of the complexes are compiled in Table 6.

Perusal of Figure 7 reveals that covalent interactions play a prominent role in the bonding mechanism of the cation−π interaction for the H^+ and Ag^+ electrophiles. In the case of the $[\{cyclo\text{-}Au_3(CH_3)_3\}H]^+$ molecule the largest contribution to the bonding scheme of the H^+−π interactions comes from the in-phase orbital interactions of the cyclically delocalized σ-, π-, and δ-MOs of the aromatic Au_3 ring with the 1s AO of the proton. These interactions described by the HOMO-2, HOMO-14, HOMO-17, HOMO-22, and HOMO-23 orbitals support a significant charge transfer of 1.08 |e| of natural charge from the aromatic Au_3 ring toward the coordinated H^+ center which acquires negative natural charge of −0.09 |e|.

For the $[\{cyclo\text{-}Au_3(CH_3)_3\}H]^+$ and $[\{cyclo\text{-}Au_3(CH_3)_3\}_2Ag]^+$ molecules the largest contribution to the bonding scheme of the Ag^+−π interactions comes from the in-phase orbital interactions of the cyclically delocalized σ-, π-, and δ-MOs of the aromatic Au_3 ring with the 4d AOs of Ag^+. Some of the relevant molecular orbitals for the sandwichlike $[\{cyclo\text{-}Au_3(CH_3)_3\}_2Ag]^+$ compound are shown pictorially in Figure 7. Interestingly, all these orbitals closely resemble those of the metallocenes, thus highlighting further the aromaticity of the Au_3 rings. The aromatic ring-to-cation charge transfer (ARMCT) amounts to 0.25 and 0.51 |e| of natural charge for $[\{cyclo\text{-}Au_3$-

(58) Amicangelo, J. C.; Armentrout, P. B. *J. Phys. Chem. A* **2000**, *104*, 11420.
(59) Ma, J. C.; Dougherty, D. A. *Chem. Rev.* **1997**, *97*, 1303.
(60) Clark, T.; Weiss, R. *J. Org. Chem.* **1980**, *45*, 1790.
(61) Wannere, C. S.; Corminboeuf, C.; Wang, Z.-X.; Wodrich, M. D.; King, R. B.; Schleyer, P. v. R. *J. Am. Chem. Soc.* **2005**, *127*, 5701.

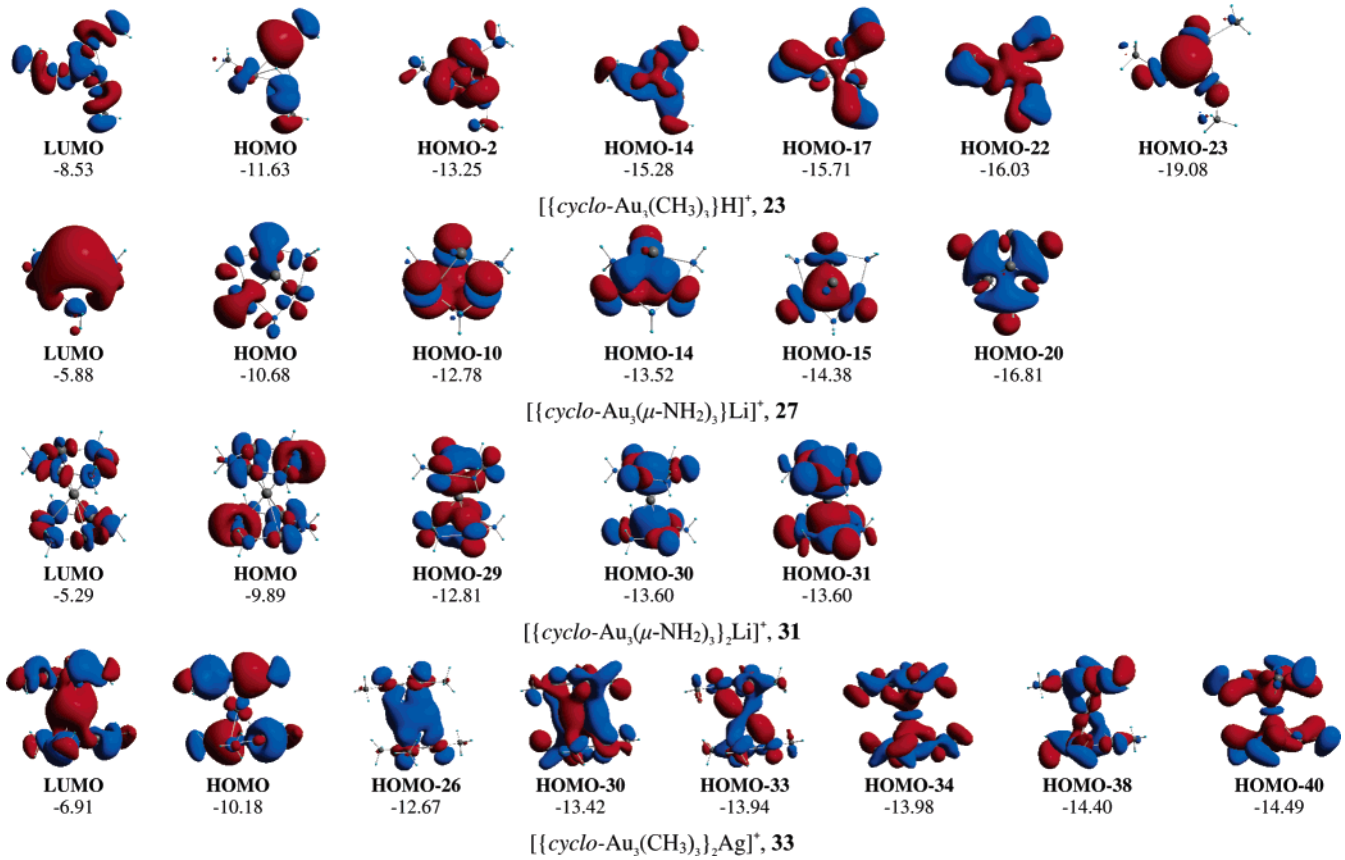

Figure 7. Most relevant valence molecular orbitals of representative $[\{cyclo\text{-}Au_3(L)_3\}_2M]^+$ and $[\{cyclo\text{-}Au_3(L)_3\}M]^+$ complexes (isocontour value of 0.01 au; eigenvalues in eV).

$(CH_3)_3\}Ag]^+$ and $[\{cyclo\text{-}Au_3(CH_3)_3\}_2Ag]^+$ complexes, respectively. It should be noted that the ARMCT renders the aromatic Au_3 rings much more electrophilic; the electrophilicity index ω values range from 6.39 to 16.38 eV (Table 6).

Inspection of the molecular orbitals describing the $Li^+-\pi$ and $Tl^+-\pi$ interactions reveals that there are no in-phase orbital interactions of the cyclically delocalized σ-, π-, and δ-MOs of the aromatic Au_3 ring with the appropriate AOs of the metal cations (Figure 7). Therefore, the bonding scheme describing the $Li^+-\pi$ and $Tl^+-\pi$ interactions seems to be dominated by electrostatic (Coulombic) interactions. A clear indication that electrostatics play the dominant role in the 1:1 $Li^+-\pi$ and $Tl^+-\pi$ interactions comes from the marginal electronic reorganization of the cations. Thus the natural electronic configuration of the Li^+ and Tl^+ cations remains essentially unchanged upon coordination; the transferred electron density to Li^+ and Tl^+ cations was found to be 0.10 and 0.18 |e|, respectively. However, in the sandwichlike 2:1 complexes there is a significant ARMCT amounting to 0.35 and 0.41 |e| for the Li^+ and Tl^+ cations, respectively. Notice that the transferred electron density is accumulated on the 2s and 6p AOs of the Li^+ and Tl^+ cations, respectively (Table 6), and therefore week covalent interactions could be supported as well.

The harmonic vibrational frequencies of the most characteristic infrared active vibrational modes associated with the M^+ vibrations in the $[\{cyclo\text{-}Au_3(L)_3\}M]^+$ and $[\{cyclo\text{-}Au_3(L)_3\}_2M]^+$ (L = CH_3, NH_2; M = H, Ag, Li, Tl) compounds are given in Table 7. The unscaled harmonic vibrational frequencies and the IR intensities computed at the B3LYP/

Table 7. Harmonic Vibrational Frequencies (cm^{-1}) of the Vibrational Modes Associated with the M^+ Vibrations along with the Absolute Shielding Tensor Elements (σ^{iso}, ppm) of the M^+ Central Atom and the NICS(0) Values (ppm) of the Coordinated Aromatic Three-Membered Gold(I) Rings for the $[\{cyclo\text{-}Au_3(L)_3\}M]^+$ and $[\{cyclo\text{-}Au_3(L)_3\}_2M]^+$ (L = CH_3, NH_2; M = H, Ag, Li, Tl) Compounds, Computed at the GIAO/B3LYP/LANL2DZ+*f*(Au)∪6-31G**(L) Level of Theory

	frequency[a]			
cluster	$\nu_{\parallel}$	$\nu_{\perp}$	σ^{iso} (M^+)[a]	NICS(0)
$[\{cyclo\text{-}Au_3(CH_3)_3\}H]^+$, **23**	557.1 574.7	906.4	22.7	−15.5
$[\{cyclo\text{-}Au_3(CH_3)_3\}Ag]^+$, **24**	43.6 44.2	138.6	271.5	−15.7
$[\{cyclo\text{-}Au_3(CH_3)_3\}Li]^+$, **25**	154.6 157.2	331.2	91.5	−17.7
$[\{cyclo\text{-}Au_3(CH_3)_3\}Tl]^+$, **26**	27.9 29.7	60.0	141.7	−18.5
$[\{cyclo\text{-}Au_3(\mu\text{-}NH_2)_3\}Li]^+$, **27**	188.7 191.1	322.5	90.4	−4.7
$[\{cyclo\text{-}Au_3(\mu\text{-}NH_2)_3\}Tl]^+$, **28**	34.5 34.8	62.2	141.6	
$[\{cyclo\text{-}Au_3(CH_3)_3\}_2Li]^+$, **29**	178.0 180.8	399.8	91.4	−17.7
$[\{cyclo\text{-}Au_3(CH_3)_3\}_2Tl]^+$, **30**	24.2 24.9	27.5	135.0	−18.6
$[\{cyclo\text{-}Au_3(\mu\text{-}NH_2)_3\}_2Li]^+$, **31**	201.5 208.0	376.6	90.1	−5.7
$[\{cyclo\text{-}Au_3(\mu\text{-}NH_2)_3\}_2Tl]^+$, **32**	31.6 32.4	58.1	134.9	−5.9
$[\{cyclo\text{-}Au_3(CH_3)_3\}_2Ag]^+$, **33**	48.5 49.5	154.1	229.9	−17.1

[a] The absolute shielding tensor elements of the free M^+ cations are 95.1, 165.9, and 312.5 ppm for Li^+, Tl^+, and Ag^+, respectively.

Scheme 5

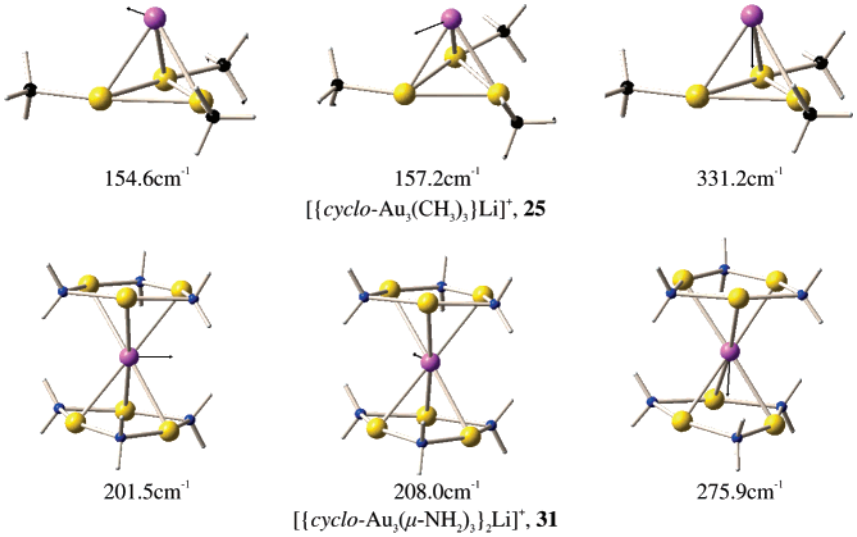

LANL2DZ+*f*(Au)∪6-31G**(L) level of theory are listed in detail in the Supporting Information (Tables S3 and S4). The absolute shielding tensor elements (ppm) of the M^+ central atom and the NICS(0) values of the coordinated aromatic three-membered gold(I) rings are also given in Table 7.

There are two kinds of vibrations associated with the coordinated M^+ atom, namely the vibration of the M^+ atom along the C_3 axis ($\nu_\perp$ vibration) and the vibration along a line parallel to the aromatic ring planes ($\nu_{||}$ vibration). The normal coordinate vectors (arrows) of representative $\nu_\perp$ and $\nu_{||}$ vibrations are shown in Scheme 5.

As expected the $\nu_\perp$ and $\nu_{||}$ vibrational modes absorb at lower frequencies as the atomic mass of M^+ increases following the trend: $H^+ > Li^+ > Ag^+ > Tl^+$. Moreover, except the Tl^+ complexes, the $\nu_\perp$ and $\nu_{||}$ harmonic vibrational frequencies are higher in the sandwichlike 2:1 than the 1:1 complexes. The $\nu_\perp$ and $\nu_{||}$ harmonic vibrational frequencies of Tl^+ complexes remain almost unchanged, thus demonstrating the dominant role of the electrostatic interactions in both the 2:1 and 1:1 complexes.

The computed NICS(0) values of the $[\{cyclo\text{-}Au_3(L)_3\}M]^+$ and $[\{cyclo\text{-}Au_3(L)_3\}_2M]^+$ (L = CH_3, NH_2; M = H, Ag, Li, Tl) compounds (Table 7) illustrate that the aromatic Au_3 rings keep their aromaticity upon complex formation. However, the aromatic character of the coordinated aromatic Au_3 rings is slightly reduced with respect to the free ligand, as it is the case for the $M_2[(GaH_3]$ compounds.[56] Interestingly, the decrease of the NICS(0) values upon complex formation is compatible with the magnitude of the ARMCT in the complexes, thus further elucidating the nature of the cation−π interactions of the complexes.

Finally, it is important to be noted that the relative changes in the shielding tensor elements of the coordinated M^+ with respect to the "free" M^+ cations can also be used to judge the aromatic character of the novel aromatic Au_3 rings. An appreciable diatropic ring current should lead to a reduced magnetic field strength and hence to an upfield shift for the cations positioned along the C_3 axis of the complexes. This is indeed the case, which further corroborates the aromaticity of the novel ligand-stabilized Au_3 rings. The chemical shifts of the coordinated M^+ cations are shifted upfield by 3.6−5.0 ppm for Li^+, 41.0 and 82.6 ppm for the 1:1 and 2:1 complexes of Ag^+, respectively, and 24.3 and 31.0 ppm for the 1:1 and 2:1 complexes of Tl^+, respectively.

Concluding Remarks

In this paper we have demonstrated, using electronic structure calculation methods (DFT), that ligand-stabilized three-membered gold(I) rings exhibit remarkable aromaticity, which is primarily due to 6s and 5d cyclic electron delocalization over the triangular Au_3 framework (s- and d-orbital aromaticity).

The results can be summarized as follows:

The novel *cyclo*-$Au_3L_nH_{3-n}$ (L = CH_3, NH_2, OH, and Cl; n = 1, 2, 3) molecules are predicted to adopt planar structures, which are characterized by perfect equalization of all metal−metal bonds in the aromatic metallic rings for the fully substituted derivatives.

A thorough search of the potential energy surfaces (PES) revealed that all *cyclo*-$Au_3L_nH_{3-n}$ clusters, except the methyl-substituted derivatives, are fluxional molecules adopting two different configurations with respect to the bonding mode of the stabilizing ligands. The global minima correspond to the structures involving bridging stabilizing ligands L, while the structures involving terminal stabilizing ligands correspond to local minima. The higher stability of the trinuclear gold(I) clusters involving symmetrical peripheral bridges around the Au_3 triangle is due to the significant aromatic character of the peripheral isosceles triangles formed. The aromatic stabilization energy based on the fully substituted *cyclo*-$Au_3(\mu\text{-}L)_3$ clusters was predicted to be 17.3, 10.1, and 13.3 kcal/mol per peripheral ring for the amido-, hydroxo-, and chloro-bridged derivatives, respectively.

All *cyclo*-$Au_3L_nH_{3-n}$ molecules are predicted to be bound with respect to their dissociation either to the AuL and/or AuH monomers or to free M, L, and H moieties in their ground states. Moreover, the computed heat of formation of the *cyclo*-Au_3L_3 species from Au(g) and L_2(g) indicated that all formation processes are exothermic; thereby strong evidence is provided that these species could be formed in MS of gold vapor sputtered with ethane, hydrazine, hydrogen peroxide, and chlorine or by the normal spectroscopic approach of deposition of the metal in an ethane, hydrazine, hydrogen peroxide, and chlorine matrix.

Considering the unusual abundance of ligand-stabilized cyclic trinuclear gold(I) complexes involving three-membered gold(I) rings in a variety of gold(I) polynuclear complexes studied so far the novel aromatic gold(I) trinuclear clusters could be synthesized following analogous synthetic routes.

The bonding of all *cyclo*-$Au_3L_nH_{3-n}$ ($L = CH_3$, NH_2, OH, and Cl; $n = 1, 2, 3$) molecules is characterized by a common ring-shaped electron density, which is constructed by highly delocalized σ-, π-, and δ-type MOs (s- and d-orbital aromaticity).

The aromaticity of the *cyclo*-$Au_3L_nH_{3-n}$ ($L = CH_3$, NH_2, OH, and Cl; $n = 1, 2, 3$) molecules was estimated by making use the magnetic criterion of the NICS(0) parameter, the upfield changes in the chemical shifts for Li^+, Ag^+, and Tl^+ cations over the ring plane, and their interaction with electrophiles, such as H^+, Li^+, Ag^+, and Tl^+ cations. Unlike, the substituted derivatives of the cyclopropenium cation and the neutral bora-cyclopropene carbacyclic analogues, the aromatic Au_3 rings interact with the aforementioned cations affording either 1:1 or 2:1 sandwichlike complexes. In this respect, they closely resemble the behavior of the "bare" *cyclo*-$[Hg_3]^{4-}$ analogue.

Regarding the bonding mechanism describing the cation$-\pi$ interactions in the 1:1 and 1:2 complexes, it was found that covalent interactions play a prominent role in the π-complexes of H^+ and Ag^+ while electrostatic interactions are dominant in the π-complexes of Li^+ and Tl^+.

The structures predicted here await experimental verification and exploration of novel properties and applications.

Supporting Information Available: The harmonic vibrational frequencies and the IR intensities are given in Tables S1−S4. The Cartesian coordinates and energies of all stationary points are compiled in Tables S5 and S6, respectively. The most relevant molecular orbitals of the trimethyl-cyclopropenium cation and the trimethyl-bora-cyclopropene are given in Figure S1. This material is available free of charge via the Internet at http://pubs.acs.org.

JA051415T